In Medium Proton Structure Functions, SRC, and the EMC effect

Hall-B Proposal April 2015

O. Hen (contact person), W. Bertozzi, S. Gilad, and B. Schmookler
Massachusetts Institute of Technology, Cambridge, MA, USA

G. Dodge, S.E. Kuhn, and L.B. Weinstein (spokesperson)
Old Dominion University, Norfolk, VA, USA

E. Piasetzky (spokesperson), E. Cohen, M. Duer, D. Izraeli, I. Korover, J. Lichtenstadt, I. Pomerantz, and I. Yaron
Tel Aviv University, Tel Aviv, Israel

W. Brooks, and H. Hakobyan (spokesperson)
Universidad Técnica Federico Santa María, Valparaiso, Chile

D.W. Higinbotham, and S. A. Wood
Thomas Jefferson National Accelerator Facility, Newport News, VA, USA

G. Ron
Hebrew University, Jerusalem, Israel

N. Dashyan
A.Alikhanyan National Laboratory (Yerevan Physics Institute), Yerevan, Armenia

G. Gilfoyle
University of Richmond, Richmond, VA, USA

P. Markowitz
Florida International University, Miami, FL, USA

A. Beck and S. Maytal-Beck
Nuclear Research Center Negev, Beer-Sheva, Israel

D. Day, R. Lindgren and V. Sulkosky
University of Virginia, Charlottesville, VA, USA

D. Ireland, K. Livingston, D. MacGregor, B. Seitz and D. Sokhan
University of Glasgow, Glasgow, Scotland, UK

J. Bericic, T. Brecelj, M. Mihovilovic, S. Stajner and S. Sirca
Jozef Stefan Institute and University of Ljubljana, Ljubljana, Slovenia

F. Benmokhtar
Duquesne University, Pittsburgh, PA, USA

Theoretical support:

M. Sargsian
Florida International University, Miami, FL, USA

W. Cosyn, and J. Ryckebusch
Ghent University, Ghent, Belgium

C. Ciofi degli Atti
INFN and Department of Physics, University of Perugia, Perugia, Italy

M. Strikman
Pennsylvania State University

L. Frankfurt
Tel Aviv University, Tel Aviv, Israel

Contents

Abstract

We propose to measure the structure functions of bound protons in deuterium as a function of their initial momentum by "tagging" the deep inelastic scattering on the deuteron with high momentum recoiling neutrons emitted at large angle relative to the momentum transfer using the reaction $d(e,e'n_s)X$.

While the EMC effect has been observed many times, there is no generally accepted explanation of its origin. Many theoretical models predict that the EMC effect is due to the modification of the nucleon structure functions in the nuclear medium and that this modification increases with nucleon virtuality ($\nu = (p^\mu)^2 - m^2$). Experimental results also indicate that most of the EMC effect stems from DIS scattering on high momentum (*i.e.*, high virtuality) nucleons in the nucleus. This proposed measurement on the deuteron will clarify the relationship between modification of the structure function and nucleon virtuality, and might have important implications for understanding the EMC effect and its relation to nucleons in Short-Range Correlations (SRC).

We propose to measure the ratio of high *x*' ($x' = Q^2 / 2p^\mu q_\mu$ is the equivalent value of Bjorken *x* for scattering from a moving nucleon) to low *x*' DIS scattering from a tagged partner proton in deuterium divided by the same ratio for the untagged scattering as a function of spectator neutron momentum. This ratio should be sensitive to the modification of the proton structure functions in the medium since we expect minimal modification at low *x*' ($0.25 < x' < 0.35$) and much larger effects at high *x*' ($0.5 < x' < 0.6$).

The electrons will be detected in the CLAS12 forward detectors, covering a wide range of *x'*. The recoiling neutrons will be detected by the central neutron detector (CND), covering scattering angles of about 40° to 120°, and by a new Backward Angle Neutron Detector (BAND) located either 2 or 3.5 m from the target, covering scattering angles of 160° to 170°.

This measurement will complement an approved Hall C experiment (E12-11-107) that will measure the modified neutron structure functions with high precision, but will measure the modified proton structure functions with much lower precision.

We propose to measure $d(e,e'n_s)X$ simultaneously with electron-deuteron measurements in CLAS, including run groups F (BoNuS), and B and possibly also E (Hadronization), and D (color transparency).

I. Introduction

I.1 The EMC effect

One of the outstanding questions in nuclear physics is whether the quark structure of nucleons is modified in the nuclear medium. Evidence for nucleon modification can only come from the failure of hadronic models, models incorporating unmodified nucleons and mesons as their fundamental degrees of freedom. While the vast majority of nuclear physics experiments can be explained using hadronic models, deep inelastic scattering (DIS) measurements (see Fig. 1) of the ratio of per-nucleon DIS cross sections of nucleus A to deuterium cannot. These experiments typically measure a ratio of about 1 at x = 0.3 ($x = Q^2 / 2m\omega$ where Q^2 is the four-momentum transfer squared, ω is the energy transfer and m is the nucleon mass), decreasing linearly to a minimum at around x = 0.7 [1–7]. This minimum depends on A and varies from about 0.94 for ^{4}He to about 0.83 for ^{197}Au (see Fig. 2). This observation is known as the EMC effect. A comprehensive review of the EMC effect can be found in [8, 9] and the references therein.

There is no generally accepted explanation of the EMC effect. In general, two classes of explanations have been proposed: 1) the internal structure of the nucleon is modified by the influence of the nuclear medium or 2) effects stemming from the nuclear medium itself, such as binding energy and Fermi motion. Note that a recent publication indicates that the Coulomb field of the nucleus also plays an important role [10].

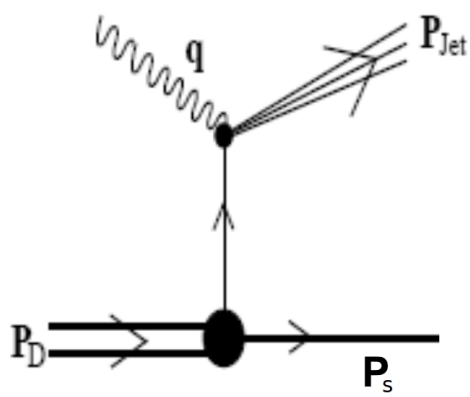

Figure 1: Deep inelastic scattering from deuterium showing the momentum transfer and the momentum of the recoil spectator.

There are many models of nucleon modification used to explain the EMC effect [8,9]. For example Kulagin and Petti [11,12] include nuclear shadowing, Fermi motion and binding, nuclear pion excess and a phenomenological off-shell correction to bound nucleon structure functions. They assumed that the off-shell correction is proportional to the nucleon virtuality $v = (p^\mu)^2 - m^2$ and parametrized it as a third-order polynomial in x. Fig. 2 shows that they cannot describe data without the offshell correction and that their full calculation describes the data very well over a wide range of x.

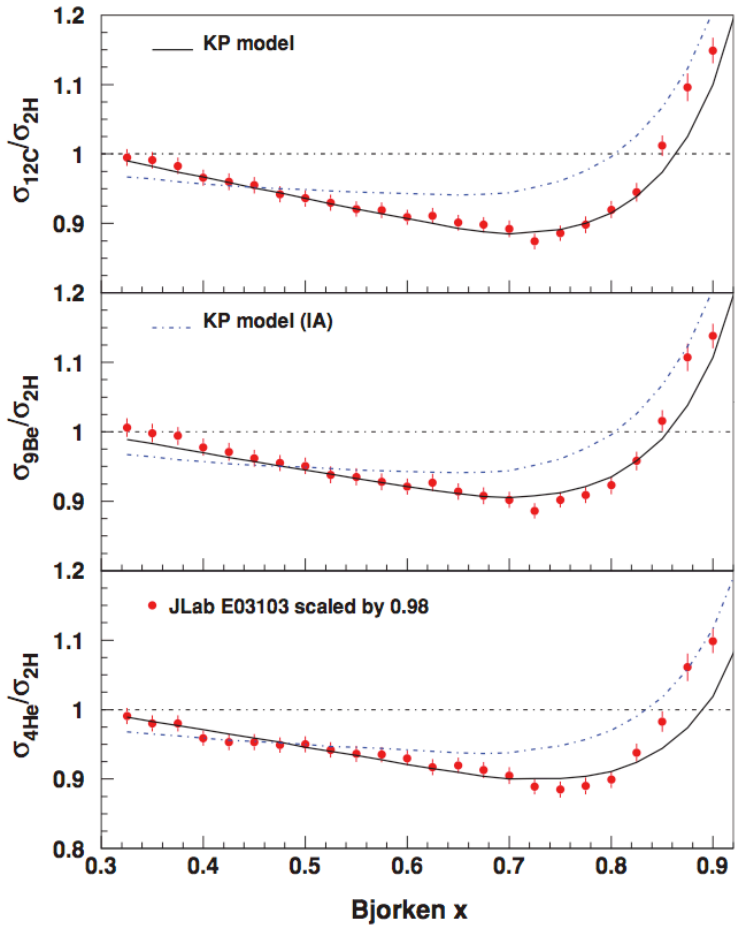

Figure 2: The per-nucleon DIS cross section ratio of ^{12}C, ^{9}Be, and ^{4}He to deuterium as a function of x. The points are from Seely [7] and the curves are from Kulagin and Petti [11,12]. The solid curve shows the full model and the dot-dashed curve shows the result with no off shell correction.

Measurements of the EMC effect on light nuclei at JLab [7] show that the EMC effect does not depend directly on the atomic mass A or the average nuclear density, as was previously assumed by some models. Beryllium is the most significant outlier (see Fig. 3). The authors claim, "The data … suggest that the nuclear dependence of the quark distributions may depend on the local nuclear environment". These data suggest that nucleon modification increases with local nuclear density. This implies that we should compare the EMC effect to other density-related nuclear phenomena such as short-range correlations.

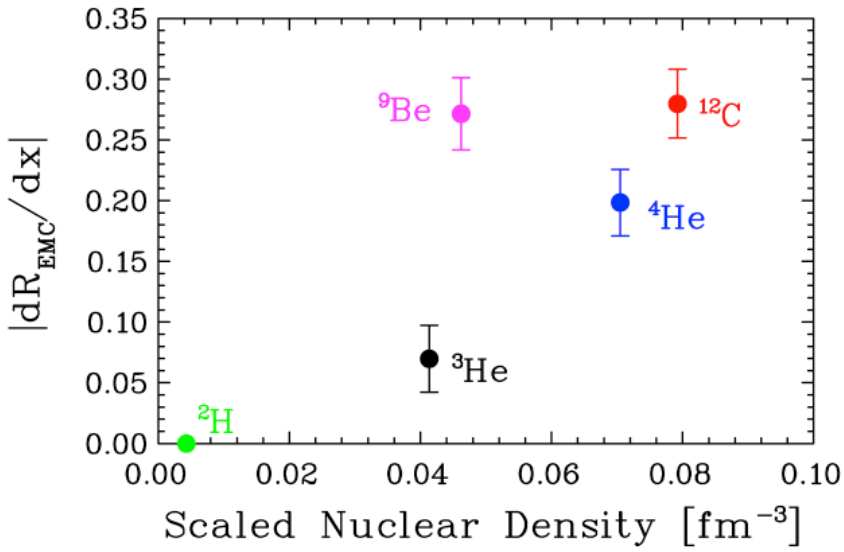

Figure 3: The slope of the EMC ratios for light nuclei from Seely [7] plotted vs the scaled average nuclear density.

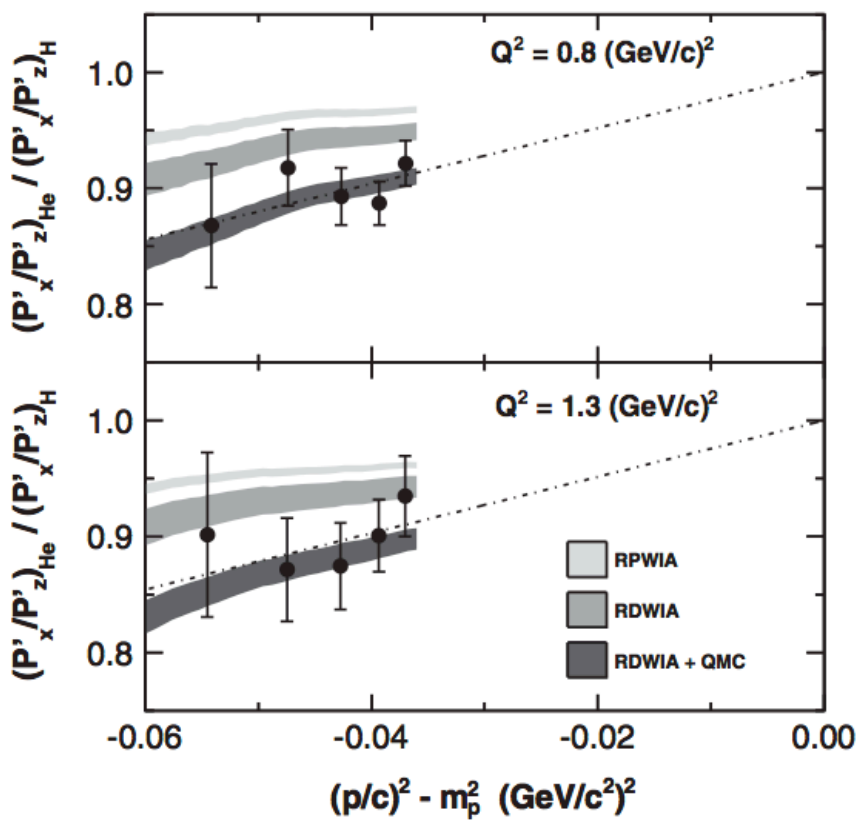

Figure 4: The double ratio of proton polarization in the *x*' and *z*' directions for $^4\mathrm{He}(\vec{e},e'\vec{p})^3\mathrm{H}$ relative to $\mathrm{H}(\vec{e},e'\vec{p})$ plotted versus nucleon virtuality showing deviation from the free nucleon for Q^2 = 0.8 and 1.3 GeV^2 [13].

Another recent JLab measurement seems to indicate that the medium modifications of the proton electromagnetic form factors increase with nucleon virtuality [13]. Proton recoil polarization was measured in the quasielastic $^4\mathrm{He}(\vec{e},e'\vec{p})^3\mathrm{H}$ reaction at Q^2 = 0.8 GeV^2 and 1.3 GeV^2. The polarization-transfer coefficients were found to differ from those of the $\mathrm{H}(\vec{e},e'\vec{p})$ reaction as the virtuality of the proton increases (see Fig. 4). Note that this experiment only explored relatively small nucleon virtualities, since the proton momenta were significantly below the Fermi momentum.

I.2 Short Range Correlation (SRC) in nuclei

Only about 60-70% of nucleons in nuclei are in single-particle mean-field orbitals. Some nucleons are in long-range correlated pairs and the rest of the nucleons are in short-range correlated (SRC) *NN* pairs. These SRC pairs are characterized by a large relative momentum and small center-of-mass momentum, where large and small are relative to k_F, the Fermi momentum of medium and heavy nuclei [14–16]. In other words, when a nucleon belongs to an SRC pair, its momentum is balanced by one other nucleon, not by the $A-1$ other nucleons.

We have learned a large amount about these correlated pairs in the last decade from experiments at Jefferson Lab [17-24, 47-48] and BNL [25-28]:

● The probability for a nucleon to belong to an SRC pair ranges from 5% in deuterium to about 25% in nuclei such as carbon and iron;

● The threshold momentum of nucleons in SRC pairs is $p_{\mathrm{thresh}} = 275 \pm 25$ MeV/c;

● The momentum distribution for $p > p_{\mathrm{thresh}}$ is the same for all nuclei, only the magnitude varies. This magnitude is expressed as a scale factor, $a_{2\mathrm{N}}$;

● Almost all nucleons with momenta greater than p_{thresh} are part of *NN*-SRC ($92 \pm 18\%$);

● These SRC pairs move inside the nucleus with c.m. motion of σ~0.14 GeV/c;

● The *NN*-SRC consists of about 90% *np* pairs, and 5% each *pp* and *nn* pairs, even in heavy asymmetric nuclei;

● The tensor force dominates *NN*-SRC for pair relative momenta $0.3 < p_{\mathrm{rel}} < 0.5$ GeV/c

● 80% of the kinetic energy (momentum) of all the nucleons in the nucleus is carried by members of the *NN*-SRC (which are only 20% of the nucleons).

A pie chart that represents our 'standard' picture of ^{12}C short range structure is shown in Fig 5.

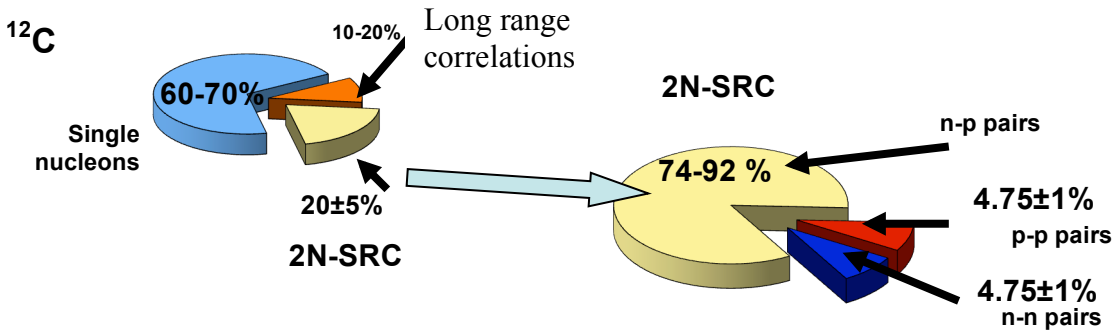

Figure 5: The short distance structure of ^{12}C as deduced from recent measurements.

I.3 SRC and the EMC effect

The size of the EMC effect in a given nucleus is linearly correlated with the probability for a nucleon in that nucleus to belong to an *NN* SRC pair (see Fig. 6) [29,49]. The dependence of the EMC effect on high momentum nucleons was first proposed in [30]. This strongly suggests that the EMC effect is due to high momentum nucleons in nuclei. Since almost all high-momenta nucleons in nuclei belong to SRC nucleon pairs, we can select the nucleons on which we observe the EMC effect by detecting their SRC partners that recoil backwards in coincidence with the scattered electrons.

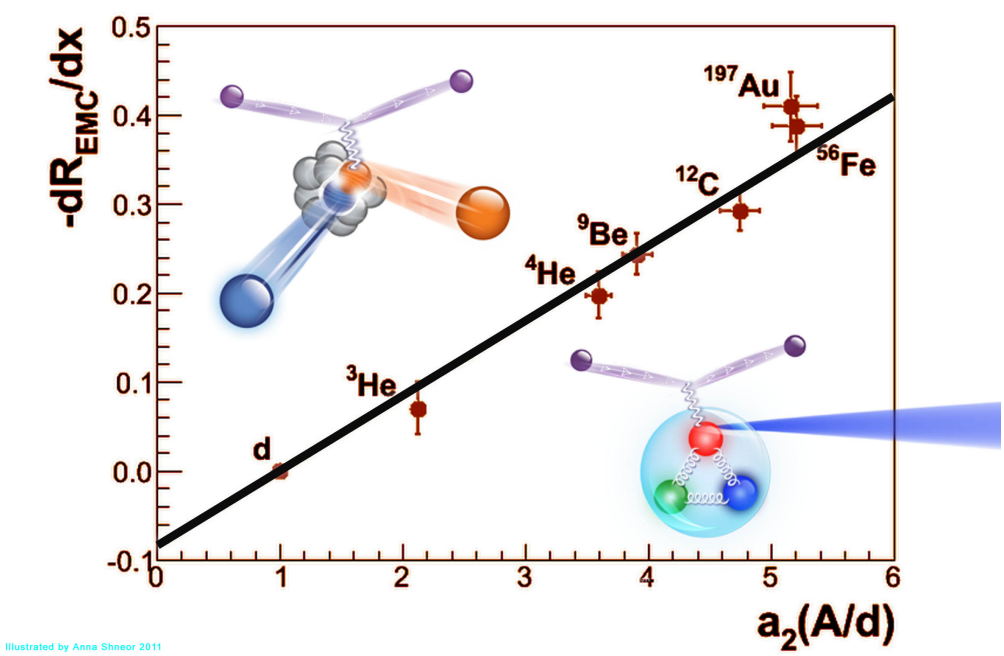

Figure 6: The negative of the EMC slope plotted vs. the relative probability that a nucleon belongs to an *NN* SRC pair for a variety of nuclei (see details in [29, 49]).

I.4 DIS off nuclei in coincidence with high momentum recoil nucleons

If the EMC effect is predominantly associated with 2N-SRC pairs in nuclei, then the per-nucleon ratio of the tagged DIS cross sections for d and nucleus A (the "tagged" EMC ratio) should be almost independent of x and larger than unity. This is because, in both nuclei, the spectator backward nucleon tags the reaction so that the electron is scattering from a high momentum forward-going nucleon. Thus, the electron is scattering from nucleons with the same momenta and virtuality in both nuclei. If the nucleon modification and hence the EMC effect depend on the virtuality of the struck nucleon rather than on the nuclear density, the per-nucleon cross section ratio (the EMC ratio) of the two nuclei should be independent of x. The magnitude of the ratio should equal the relative probabilities for a nucleon to belong to a SRC pair in those two nuclei.

Fig. 7 shows an analysis of CLAS EG2 5 GeV data by Barak Schmookler. The data have been corrected for radiative and acceptance effects. The left plot shows the EMC ratio of the per-nucleon DIS (e,e') cross-sections for C and deuterium for $Q^2 > 1.25$ GeV^2 and $W > 2$ GeV. It agrees with previous results and shows the typical linear decrease in the ratio from $x = 0.3$ to $x = 0.5$ (at this beam energy, requiring $W > 2$ GeV limits the maximum x to about 0.5). Even at these low values of Q^2 higher twist effects should cancel in the EMC ratio. The right plot shows the tagged EMC ratio, requiring that a high momentum proton ($p > 0.3$ GeV/c) be detected at an angle greater than 120° degrees from the momentum transfer. The results are approximately constant with x and the value of the ratio is 5.1 ± 0.6, consistent with the expected ratio of $a_{2N}(\mathrm{C}/d) = 4.65 \pm 0.14$ [49]. This agreement may be fortuitous, since the tagged EMC ratios have not been corrected for final state interactions of the outgoing proton, which should be significantly larger in carbon than in deuterium.

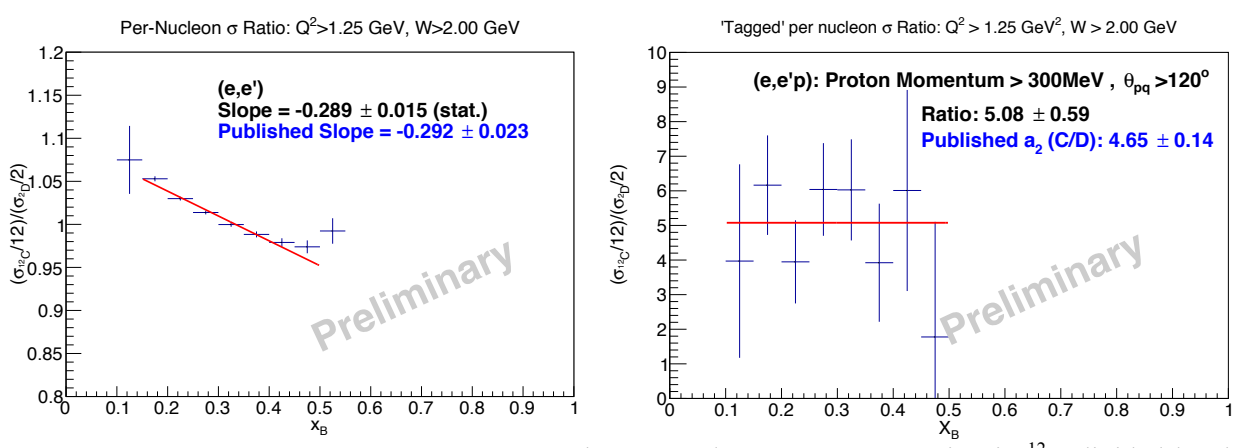

Figure 7: Preliminary and not for release. The per-nucleon DIS cross-section in ^{12}C divided by the same quantity for the deuteron. Left: untagged inclusive cross-section; Right: the cross section tagged by a high momentum, $p > 0.3$ GeV/c, backward proton. The data are a preliminary analysis of CLAS data by B. Schmookler.

While it would be premature to draw quantitative conclusions from this preliminary data, the tagged EMC ratio is clearly very different from the untagged data and agrees with our simple SRC-correlated virtuality-dependent EMC effect idea.

I.5 DIS off the Deuteron in coincidence with high momentum recoil nucleons

Due to the lack of a free neutron target, the EMC measurements used the deuteron as an approximation to a free proton plus neutron system and measured the ratio of inclusive DIS on nuclei to that of the deuteron. This seems like a reasonable approximation since the deuteron is loosely bound (≈ 2 MeV) and the average distance between the nucleons is large (≈ 2 fm). But the deuteron is not a free system. We define the In-Medium Correction (IMC) effect as the ratio of the DIS cross section per nucleon bound in a nucleus relative to the free *pn* pair cross section (as opposed to the EMC effect which uses the ratio to deuterium).

The deuteron IMC effect can be extracted from the data in Fig. 6. If the EMC/IMC effect and the SRC scaling factor both stem from the same cause, then the IMC effect and the SRC scaling factor, $a_{2N}(A/d)$, will both vanish at the same point. The value $a_{2N}(A/d) = 0$ is the limit of free nucleons with no SRC. Extrapolating the best fit line in Fig. 6 to $a_{2N}(A/d) = 0$ gives a y-intercept of $dR_{EMC}/dx = -0.084 \pm 0.004$. The difference between this value and the deuteron EMC slope of 0 is the deuteron IMC slope. Following [29,49] the expected IMC effect on a deuteron at x=0.6 is about:

$$\frac{\sigma_d}{\sigma_p + \sigma_n} = 1 - (0.084 \pm 0.004)(0.6 - 0.31 \pm 0.04) \approx 0.975$$

where 0.084 is the expected EMC slope for the ratio of a free proton plus neutron to deuterium, and (0.6 – 0.31) is the difference in x from 0.31 (where the EMC effect is zero) to x = 0.6. Thus we expect that the deuteron DIS cross-section at x = 0.6 is 2.5% smaller than the sum of the proton plus neutron DIS cross sections at x = 0.6.

If the dominant contribution to the IMC effect is due to the high momentum tail nucleons, then this 2.5% effect is due to the 5% of nucleons with $p > p_{\text{thresh}} \approx 275$ MeV/c. Therefore we expect that the modification of these high-momentum nucleons to be of the order:

$$\frac{\sigma_p^*}{\sigma_p} \approx \frac{\sigma_n^*}{\sigma_n} \approx \frac{2.5\%}{5\%} \approx 50\%$$

where σ_p^* and σ_n^* are the medium-modified high-virtuality DIS cross sections and the probability of finding a nucleon with $p >$ 275 MeV/c in the deuteron is about 5%. This is a qualitative argument that neglects effects such as Fermi motion. However, it should indicate the order-of-magnitude of the effect.

Deuterium is the optimal system in which to study the dependence of the nucleon structure on the nucleon virtuality. The probability for a high momentum configuration in the deuterium is rather small relative to heavier nuclei but this configuration can be 'tagged' cleanly by the emission of a fast nucleon to the backward hemisphere. In a simple spectator picture with no FSI the backward moving nucleon is a spectator, does not participate in the DIS process, and allows us to determine the virtuality of the nucleon from which the electron scattered. The effect of FSI will be discussed in section II.3 below.

II. Theoretical Background

II.1 The Formalism for inclusive and semi-inclusive DIS

The inclusive cross section for an electron scattering off a free nucleon at rest in the laboratory frame can be expressed in the DIS region in terms of the structure functions F_1 and F_2:

$$\frac{d^3\sigma}{d\Omega dE'} = \left(\frac{d\sigma}{d\Omega}\right)_{Mott} \cdot \left[\frac{1}{\omega}F_2(x_B,Q^2) + \frac{2}{M}F_1(x_B,Q^2)\cdot\tan^2(\theta_e/2)\right],$$

where the Mott cross section is the cross section to scatter off a point charge, θ_e is the electron scattering angle in the lab frame, Q^2 is the four momentum transfer, and x is the Bjorken scaling variable given by:

$$x = \frac{Q^2}{2M\omega}.$$

The structure functions F_1 and F_2 are related by $R(x,Q^2)$, the ratio between the cross sections for longitudinal and transverse scattering. Using the measured values of R, F_2 can be extracted from the measured cross section:

$$F_2(x,Q^2) = \left[\frac{d^2\sigma/d\Omega dE'}{(d\sigma/d\Omega)_{Mott}}\right]\cdot\left[\frac{\omega\varepsilon(1+R(x,Q^2)}{1+\varepsilon R(X,Q^2)}\right],$$

where the polarization of the virtual photon is: $\varepsilon = [1+2(1+Q^2/(4M^2))\tan^2(\theta_e/2)]^{-1}$.

When scattering off a nucleon in a nucleus, the movement of the nucleon needs to be taken into account. For a free nucleon moving in the lab frame, the Bjorken scaling parameter is

$$x' = \frac{Q^2}{2p_\mu q^\mu},$$

where p_μ and q_μ are the four vectors of the struck nucleon and the virtual photon respectively. For a nucleon at rest $p_\mu = (M,\vec{0})$ and $x' = x$.

In a deuteron, x' can be expressed in terms of the measured recoil tagged nucleon:

$$x' = \frac{Q^2}{2[(M_d - E_s)\omega + \vec{p}_{s\cdot}\cdot\vec{q}]},$$

where E_s is the energy of the recoil nucleon and $\vec{p}_s$ and $\vec{q}$ are the three-momenta of the recoil nucleon and virtual photon respectively. Note that $\vec{p}_s\cdot\vec{q} < 0$ since $\theta_{qs} > 90^o$ and hence $x' > x$.

The total hadronic mass squared for a free nucleon at rest is: $W^2 = M^2 - Q^2 + 2M\omega$. The total hadronic mass for a moving nucleon absorbing a virtual photon in deuterium can also be written in terms of the recoil spectator momentum:

$$W'^2 = (q^\mu + p_d^\mu - p_s^\mu)^2,$$

where $p_d^\mu = (M_d,\vec{0})$ is the 4-momentum of the deuteron (here we are being a little careless about the difference between covariant and contravariant four-momenta). This gives:

$$W'^2 = m^2 - Q^2 + 2\omega(M_d - E_s) + 2\vec{p}_s \cdot \vec{q} = m^2 - Q^2 + 2\omega(M_d - E_s) + 2p_s\sqrt{Q^2+\omega^2}\cos(\theta_{sq}),$$

where θ_{sq} is the angle between the virtual photon and the recoil nucleon and

$$|\vec{q}| = \sqrt{Q^2+\omega^2}.$$

To ensure a DIS process, we require for the moving nucleon:

$$Q^2 \geq 2 \text{ GeV}^2$$

$$W'^2 \geq 4 \text{ GeV}^2.$$

Note that, while higher twist effects increase as Q^2 decreases, these effects mostly cancel in the ratio of cross sections. That is why EMC cross-section ratios are almost independent of Q^2 for $2 < Q^2 < 40 \text{ GeV}^2$ [3].

For a deuteron, even in the presence of FSI, the cross section for the semi-inclusive process factorizes [34,40]:

$$\frac{d^4\sigma}{dxdQ^2d\vec{p}_2d\phi_e} = KS_D(\vec{p}_s,\vec{q})F'(x',\alpha_s,p_T,Q^2),$$

where F' is the in-medium structure function of the nucleon in the deuteron, K is a kinematic factor, and S_D is the distorted deuteron momentum distribution.

The deuteron distorted momentum distribution can be expressed as a function of the measured parameters $S_D = S_D(p_s,\theta_{sq},W',Q^2)$ where the momentum distribution of the deuteron is determined by p_s and the FSI depends primarily on θ_{sq} and the invariant mass of the outgoing hadrons W'.

II.2 Off shell cross section models

Motivated in part by the EMC effect results, theorists have proposed many different models of offshell nucleons. Melnitchouk, Sargsian and Strikman [34] calculated the change in the nucleon structure function in deuterium for three different models: a Point-Like Configuration (PLC) suppression model, a binding/offshell model, and a rescaling model where the change in quark localization from the deuteron to heavy nuclei is related to a Q^2 rescaling. Fig. 8 shows the predictions for the effective proton structure function in nuclei divided by the free F_{2p} for the different models as a function of $\alpha_s = (E_s - p_s^z)/m_s$ and of x where α_s is the light cone variable, and E_s, p_s^z and m_s are the energy, component of the momentum parallel to the virtual photon, and mass of the backward spectator nucleon. At $\theta_{pq} = 180^o$, $\alpha_s = 1.5$ corresponds to $p_s^z = -0.4$ GeV/c.

Melnitchouk, Schreiber and Thomas [35,36] calculated the ratio of the bound to free neutron structure functions in a covariant model with relativistic vertex functions which parametrize the nucleon--quark-"diquark" interaction (where "diquark" just refers to a nucleon with one quark knocked out). The parametrization is constrained by fitting to on-shell structure functions. Figure 9a shows that they find much smaller effects in the ratio of F_{2n}^{eff} / F_{2n} than the previous model. The results for a similar model by Gross and Liuti [37,38] are shown in Fig. 9b. Note that they expect a much larger change in the bound nucleon structure function but a much smaller dependence on *x*.

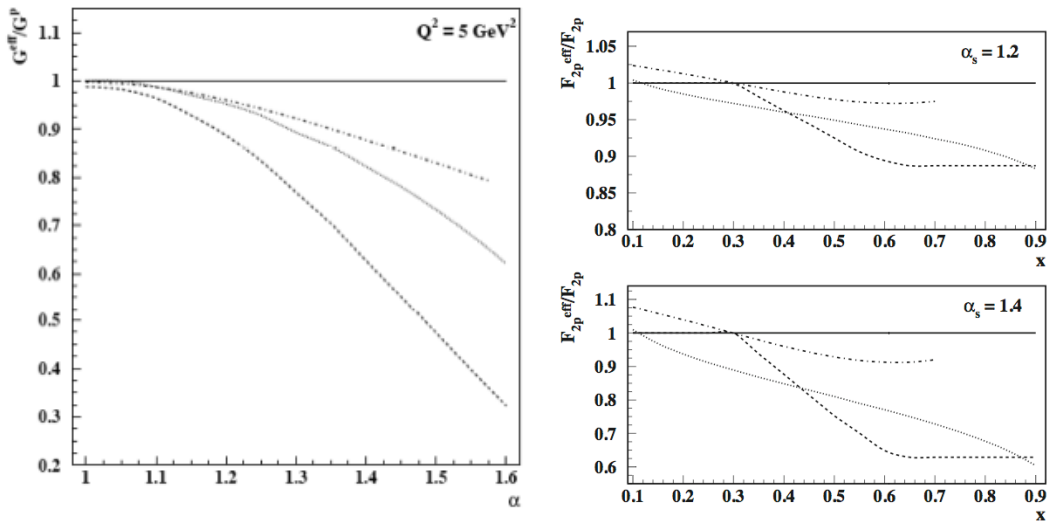

Figure 8: (left) The α dependence of F_{2p}^{eff} / F_{2p} in deuterium for $x = 0.6$, $Q^2 = 5$ GeV^2 and $p_T = 0$ ($\theta_{pq} = 180^o$) [34]. (right) The *x* dependence of F_{2p}^{eff} / F_{2p} for (upper) $\alpha_s = 1.2$ and (lower) $\alpha_s = 1.4$. The dashed line shows the PLC suppression model, the dotted line shows the rescaling model, and the dot-dashed line shows the binding/off-shell.

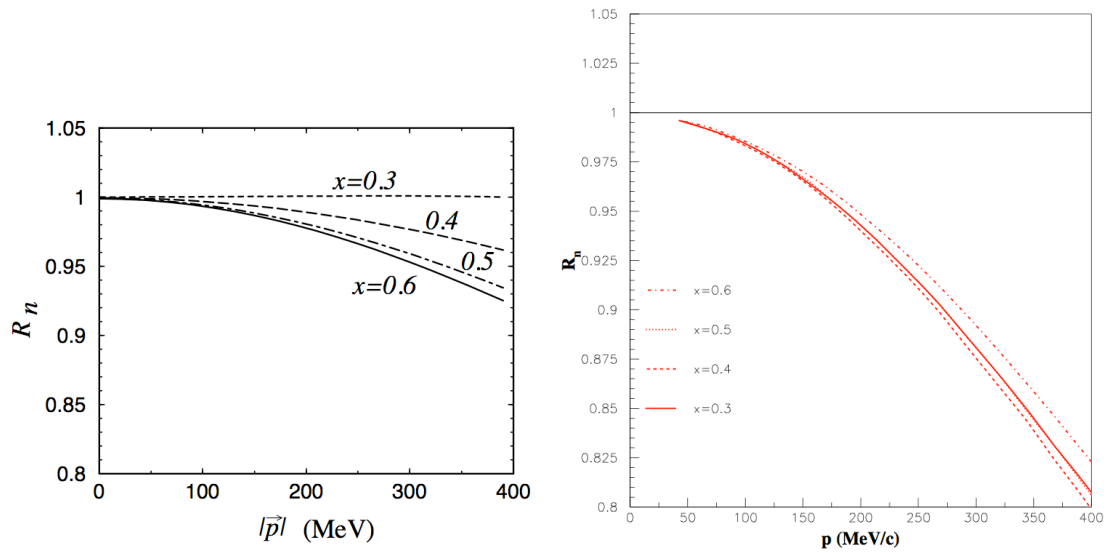

Figure 9: The dependence of the ratio $R_n = F_{2n}^{eff} / F_{2n}$ in deuterium for $Q^2 = 5$ GeV^2 as a function of spectator proton momentum in (left) the model of Melnitchouk, Screiber and Thomas [36] and (right) the model of Gross and Liuti [37,38] as shown in Ref. [39].

Because the different models predict very different α_s, p_s and x dependences, we will measure the cross section as a function of all of those variables.

II.3 Final State Interactions (FSI)

FSI are due to the interactions of the recoiling nucleon with the propagating struck nucleon debris formed after the virtual photon absorption by a quark. Note that this is complicated by propagation and hadronization of the struck quark and of the residual system.

While there is no complete theory of FSI in DIS, there are a number of phenomenological models for the deuteron. The magnitude of the FSI in the reaction $d(e,e'p_s)$ has been calculated in several models using PWIA [34], general eikonal approximation as fit to data [40], and with models for the debris-nucleon interaction cross sections [41,42]. In general, FSI are expected to be much smaller at backward angles. This decrease in FSI with angle is supported by $d(e,e'p_s)X$ data from CLAS [31]. Figure 10 shows that the PWIA spectator picture describes the data rather well for proton angles larger than 107° relative to the momentum transfer direction (panel a). On the other hand, at angles around 90° (panel b), a large excess of high-momentum protons over the PWIA spectator expectation is observed, which is most likely due to strong final state interactions.

The different model calculations agree that FSI increase with W' and decrease with Q^2. Since FSI should not depend strongly on x', the ratio of cross sections for two different value of x' should be much less sensitive to FSI.

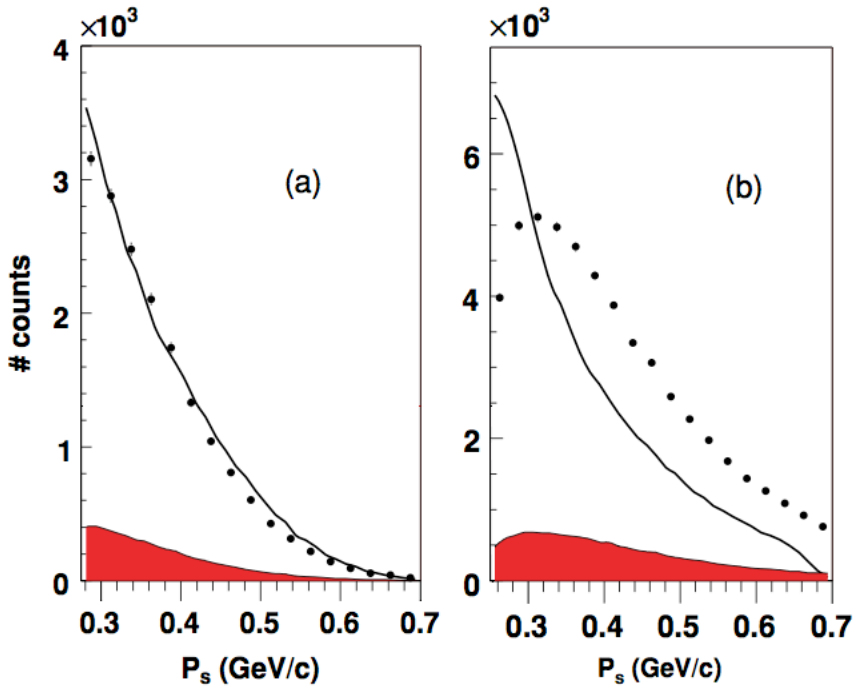

Figure 10: Momentum distribution of the recoiling proton in the reaction $d(e,e'p_s)X$ [31]. Data (points) are compared with a PWIA calculation integrated over the experimental acceptance for the range of recoil angle (a) $-1 < \cos\theta_{pq} < -0.3$ and (b) $-0.3 < \cos\theta_{pq} < 0.3$. Events were integrated over all W and Q^2.

While recent model calculations agree that FSI are smaller for backward recoil nucleons, they strongly disagree about the magnitude of the FSI. Cosyn and Sargsian [40] predict little or no FSI in the backward direction, whereas Ciofi degli Atti and collaborators [41,42] found large FSI even at backward recoil angles (depending on the kinematics).

Therefore it is important to measure ratios of cross sections at different kinematics chosen to maximize or minimize the sensitivity of the ratios to FSI.

To demonstrate the reduction in the sensitivity to FSI we can use the calculation by Ciofi [41,42] which predicts the largest backward angle FSI. According to this calculation, for $p_s = 0.3$ GeV/c, $W' = 2$ GeV^2 and $\theta_{pq} = 145^o$ the difference between the cross section with and without FSI can be as much as a factor of 2 for $x' = 0.27$ and $x' = 0.37$. However, because p_s, W' and θ_{ps} are held constant, the double ratio of the PWIA to the full calculation at these two x' values is unity to better than 1%.

We will measure cross sections over a very wide range of kinematics so that we can study the variation of FSI and other cross section ingredients with p_s, W', x', etc.

We will then determine ratios of experimental cross sections measured in kinematics such that FSI, at a given value of the recoil moment of the detected neutron (p_s), are minimized (

$\theta_{ps} > 110^o$) and relatively constant (fixed W'). These ratios at different x' will be used to measure the in medium structure functions of bound nucleons and look for their possible medium modification.

II.4 Extracting in-medium nucleon structure functions

Ideally one could measure the $d(e,e'n_s)$ cross section and extract from it the corresponding nucleon structure function, but the cross section depends upon: (i) the distorted momentum distribution, which in turn depends on the FSI in a model dependent fashion, and (ii) the in-medium structure function we want to investigate. Fortunately, one can take advantage of the fact that the tagged DIS cross section factorizes into the nucleon structure function times the distorted momentum distribution. Therefore we should choose pairs of kinematic points such that the effects of FSI and the deuteron momentum distribution cancel in the ratio of cross sections. In other words, we should measure the ratio of cross sections at kinematics which have the same p_s and W' but different x'. In this case, the cross section ratio should be very sensitive to any distortions of the in-medium nucleon structure functions. Under these conditions the theoretical corrections and hence their uncertainty will be minimized.

The ratio between the $d(e,en_s)$ cross section at two different x' values, keeping the recoil nucleon kinematics the same, is:

$$\frac{d^4\sigma}{dx_1 dQ_1^2 d\vec{p}_s} \Bigg/ \frac{d^4\sigma}{dx_2 dQ_2^2 d\vec{p}_s} = (K_1 / K_2)[F_2^*(x_1',\alpha_s,p_T,Q_1^2) / F_2^*(x_2',\alpha_s,p_T,Q_2^2)]$$

Using $x_1' \approx 0.5 - 0.6$ and $x_2' \approx 0.3$ we will measure the ratio of effective structure functions:

$$[F_2^*(x_1',\alpha_s,p_T,Q_1^2) / F_2^*(x_2',\alpha_s,p_T,Q_2^2)] = \left(\frac{d^4\sigma}{dx_1 dQ_1^2 d\vec{p}_s} / K_1 \right) \Bigg/ \left(\frac{d^4\sigma}{dx_2 dQ_2^2 d\vec{p}_s} / K_2 \right)$$

Integrating over the recoil scattering angle in the range where the FSI is expected to be small, we will compare the measured ratio as a function of α_s to the measured free proton structure function.

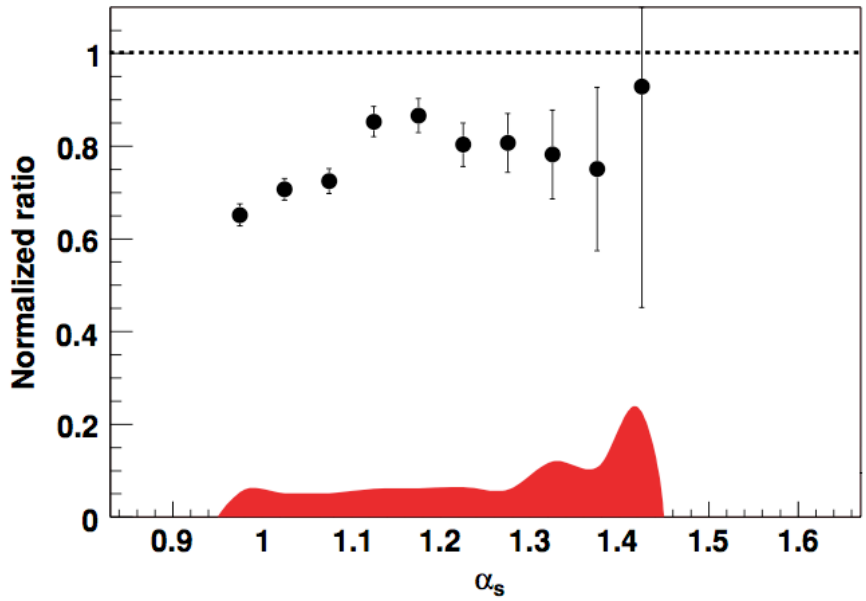

Figure 11: Ratio of the extracted off-shell structure function F_{2n} at $x' = 0.55$, $Q^2 = 2.8\,\text{GeV}^2$ to that at $x' = 0.25$, $Q^2 = 1.8\,\text{GeV}^2$, divided by the ratio of free structure functions at those kinematic points. The error bars show the statistical uncertainty; the shaded band indicates the systematic uncertainty. [31]

This ratio was already measured in the CLAS Deeps experiment [31]. Fig. 11 shows the ratio of the extracted in-medium structure function F_{2n}^{eff} at $x' = 0.55$, $Q^2 = 2.8\,\text{GeV}^2$ to that at $x' = 0.25$ $Q^2 = 1.8\,\text{GeV}^2$, divided by the ratio of free structure functions at those kinematic points (substituting *x* for *x*') for $0.25 \le p_T \le 0.35$ GeV/c plotted versus the spectator nucleon light cone fraction $\alpha_s = (E_s - p_s^z)/m$. In this ratio the effects of the deuteron momentum distribution should cancel. However, FSI do not appear to cancel. This is most apparent at $\alpha_s \approx 1$ ($\theta_{qs} \approx 90^o$) where FSI effects are largest and the ratio is smallest.

For $\alpha_s \ge 1.2$ the measured ratio is consistent with being constant. This disagrees with the more dramatic predictions shown in Figs. 8 and 9. However, due to the limited kinematic flexibility available at 6 GeV, *W*' varied with α_s. Therefore the effects of FSI probably also varied with α_s.

It is important to remeasure these ratios with enough data over a broad enough kinematic range to understand and control the Final State Interactions correction and other systematic effects.

II.5 The Hall C Experiment

This proposed measurement will complement E12-11-107, "In Medium Nucleon Structure Functions, SRC, and the EMC Effect". That experiment has been approved for 40 days of beam, using the HMS and SHMS to detect electrons (to increase the count rate) and a custom-built Large Angle Detector (LAD) to detect the recoil protons and neutrons from 85 to 175 degrees.

LAD is being built from surplus CLAS6 TOF detectors that are being refurbished at ODU. It will have an out of plane acceptance of about $\pm 20^{\circ}$ and a neutron detection efficiency of about 5% for $\theta_s < 110^o$ and about 20% for $\theta_s > 110^{\circ}$. The experiment will run at a luminosity of $2 \times 10^{36}\,\mathrm{cm}^{-2}\mathrm{s}^{-1}$. The expected results are shown in Fig. 12. This experiment will not be one of the first experiments to run in Hall C.

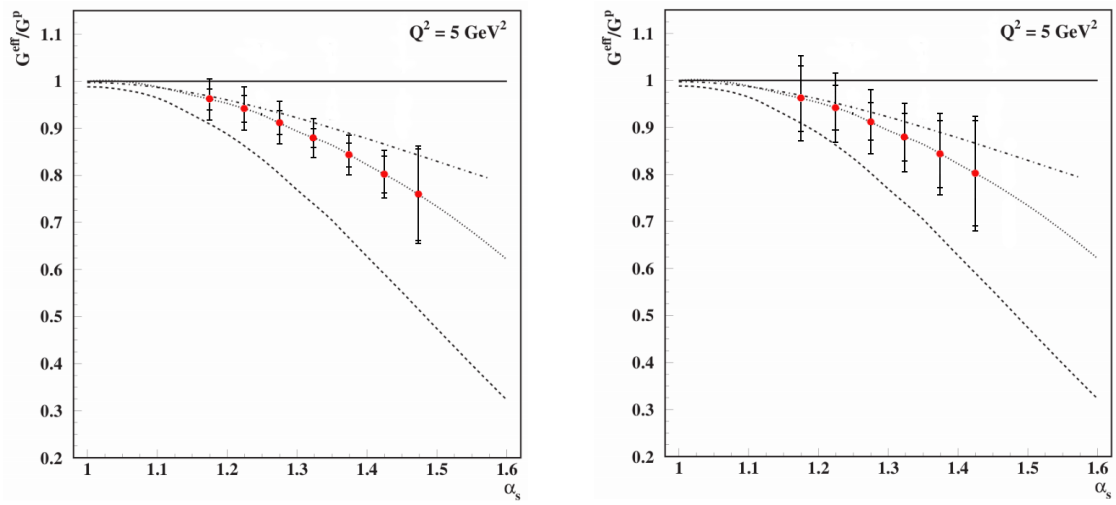

Figure 12: Expected sensitivity of the E12-11-107 experiment to the bound neutron (left) and proton (right) structure function modification $F^{eff}_{2p(n)} / F_{2p(n)}$ in deuterium as a function of α (the light-cone momentum fraction). The different lines show model calculations for x=0.6, Q^2=5 GeV^2 and p_T=0 ($\theta_{sq} = 180^0$) [32] for: Point Like Configuration (PLC) suppression model (dashed line), rescaling model (dotted line), and binding/off-shell model (dot-dashed line). The simulated data points show the expected statistical (inner error bars) and total (outer error bars) uncertainties. The left panel is for the $d(e,e'p_s)$ reaction and the right for $d(e,e'n_s)$. We expect an additional 4% interpretation uncertainty due to the effects of FSI. The label "Q^2 = 5 GeV^2" refers to the models, not the data.

II.6 Scientific Impact

The EMC/SRC correlation and the proposed new insight it offers for the cause of the EMC effect was chosen as a 'physics highlight' by the 2013 DOE NP comparative review [28] and the APS DNP 2014 town meeting [29]. The latter, together with the Jefferson Lab 12GeV white paper [30], marked the measurement of the structure of nucleons at short distance as one of the main goals of the future Jefferson Lab physics program.

The JLab Program Advisory Committee (PAC) 38 approved the complementary experiment E12-11-107 for 40 days. The internal JLab theory review, headed by Anatoly Radyushkin and Mike Pennington concluded that "This is a well motivated experiment that has to be done, and one JLab is well placed to perform".

III. Details of the proposed measurements

III.1 The Experimental Approach

The goal of the proposed experiment is to measure the in-medium proton structure function and to compare it to the free one. The obstacles to this are:

1. The deuteron wave function is not well known at the large momentum that we plan to tag the DIS with.

2. The FSI are not well known.

To overcome these obstacles we plan to:

1. Compare measured cross sections to a variety of state of the art calculations over a broad kinematical range in order to check and/or optimize the calculations.
    a. Measure cross sections at $\theta_{ps} \approx 90^o$ to study FSI,
    b. Measure cross sections at $\theta_{ps} > 140^o$ to minimize FSI,
2. Construct ratios of cross sections to reduce the systematic uncertainty of both the measurements and the theoretical calculations needed to extract the in-medium structure functions.

We propose to measure the semi-inclusive cross section with the scattered electron detected simultaneously over a range of *x*', from *x*'~0.3 where the EMC effect is negligible and little nucleon modification is expected to *x*'>0.5 where the EMC effect is large and significant nucleon modification is expected (in some models). The scattered electrons will be detected in coincidence with recoil neutrons with momentum of 300-600 MeV/c over a wide angular range $45^o < \theta_n < 120^o$ and $160^o < \theta_n < 170^o$.

III.2 Experimental setup and kinematics

We propose to perform the measurement using 10.9 GeV electrons incident on a deuteron target in CLAS12 in coincidence with a dedicated backward angle neutron detector BAND. We will require

$Q^2 \geq 2$ GeV^2

$W'^2 \geq 4$ GeV^2

$\theta_{pq} \geq 140^0$

$p_n \geq 275$ MeV/c

Fig. 13 shows the electron acceptance of CLAS12. CLAS will cover a much broader range in Q^2 and *x* than the Hall C spectrometers of E12-11-107.

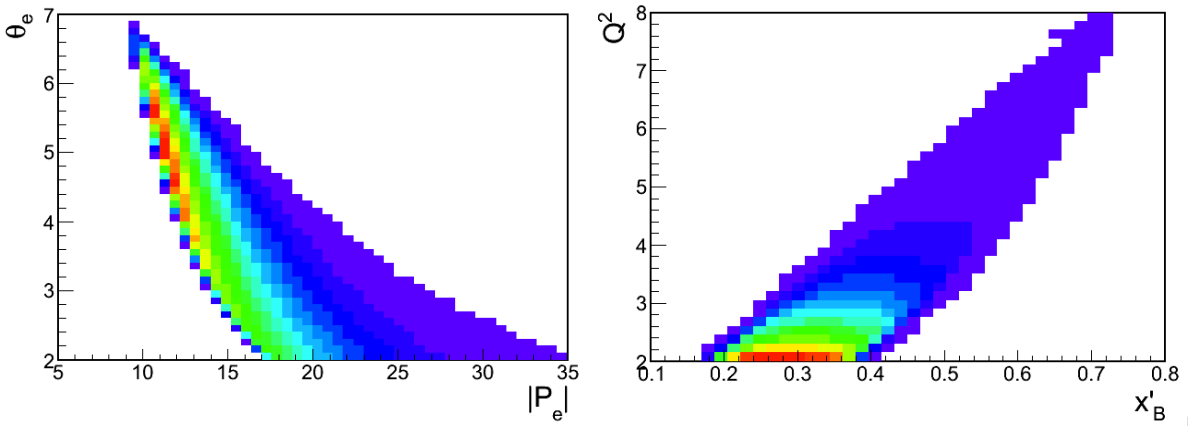

Figure 13: (left) The distribution of events in scattered electron energy *E*' and angle θ_e Events are distributed according to the cross section [40]. (right) The distribution of events in Q^2 and *x*'.

III.2.1 The BAND Detector

To detect recoil nucleons in the momentum range of 0.25 – 0.6 GeV/c, we propose to design and build a Backward Angle Neutron Detector (BAND), located 3.5 m upstream of the CLAS12 target and covering lab scattering angles from 160° to 170°, see Fig. 14. BAND will probably be constructed as a "ring" of plastic scintillators perpendicular to the beam line with inner radius of 60 cm, outer radius of 120 cm, and a thickness of 24 cm. The final thickness will be adjusted to give a 30% neutron detection efficiency with a detection threshold of 2-3 MeVee. To optimize its momentum resolution, BAND will be divided into four, 6-cm thick, layers. Each layer will be made of 75 6-cm by 60-cm scintillator strips arranged radially, tapering from 5 cm wide at *R* = 60 cm to 10 cm wide at *R* = 120 cm, see Fig. 15. An additional thin veto layer for charged particles will be placed in front. Similar to the CLAS12-CND, BAND will be read out using light-guides and PMTs. Two adjacent strips from the same layer will be read out using a common light-guide and a single PMT. The readout will be offset at the other end of the scintillators to allow identifying the specific scintillator fired. Including scintillators, light guides and PMTs, BAND will extend from 40 to 150 cm from the beam line. Table 1 shows the PMTs we plan to test for possible use in BAND. We anticipate achieving 200 ps resolution, similar to the 140-150 ps achieved by the NeuLand Collaboration at GSI and the CND group in CLAS12.

We will work with the Hall B designers and engineers to make sure that our detectors and electronics do not conflict with existing Hall B structures. The hardware and electronics readout for BAND will be supplied by our collaboration, in full coordination with the relevant Hall-B personnel. In principle BAND can be configured as added TOF counters and should therefore have no conflict with the already approved deuteron experiments.

Table 1: Properties of PMTs we will test for BAND.

Model	Rise Time [ns]	Transit Time Spread [ns]	Gain	Noise [nA]	Noise @10^6 [nA]	5% Linearity @10^6 [nA]	Comments
1" diameter							
R8619	2.5	**1.2**	2.6×10^6	2	**0.8**	5	Used by NeuLAND
R3478	1.3	**0.36**	1.7×10^6	10	**6**	5	
R6427	1.7	**0.5**	5.0×10^6	10	**2**	30	
1.5" diameter							
R7761	2.1	**0.35**	1.0×10^7	15	**1.5**	50	
2" diameter							
R10533	2	**0.28**	4.2×10^6	50	**12**	20	Used by CNB
R1828	1.3	**0.55**	2.0×10^7	50	**2.5**	25	

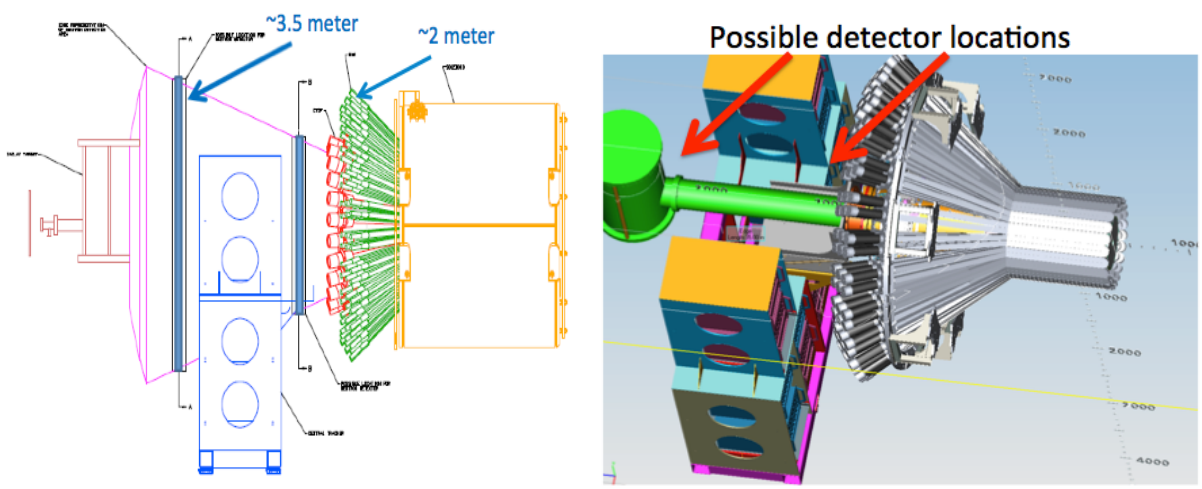

Figure 14: The preliminary design of the experimental set up for CLAS12+BAND**.** The left figure shows an elevation view of equipment racks (blue outline), light guides and phototubes of the central detectors (green and red), and the outside of the solenoid magnet (orange). Possible locations of the BAND detector are shown in solid blue. The right side shows the cryogenic system and beamline (green), the central detectors, light guides and PMTs (gray) and the equipment racks. The solenoid magnet is not shown. Red arrows indicate the possible BAND locations.

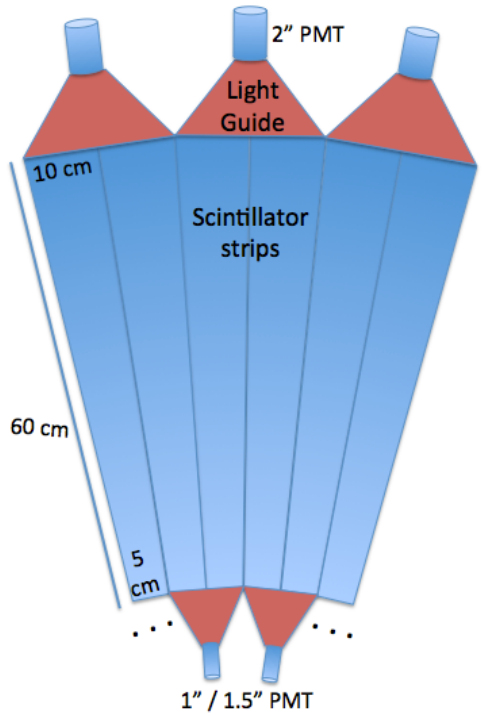

Figure 15: A schematic view of part of one layer of the BAND detector. The outer and inner ends of the scintillator strips will be read out using 2" and either 1.5" or 1" PMTs, respectively.

Neutrons leaving the target at backward angles will pass through the support structures for the central detectors. At lab angles of 170° to 163°, the neutrons will pass through a single 0.3 cm stainless steel tube. Even at these oblique angles, the effect of the support structure is small as the neutrons only pass through 1.5 cm of stainless steel. At angles of 163° to 160° the neutrons pass through ~4 cm of stainless steel. Geant4 simulations of the proposed setup indicate that the stainless steel support structure attenuates 10 - 30% of the neutrons with no effect on the momentum reconstruction using TOF.

We will use time-of-flight to identify neutrons and to determine their momentum using exactly the same technique that we used in Hall A at much higher luminosity [22,47]. Figure 16 shows the electron-neutron time in Hall A for one kinematics of the ^{4}He(e,e'pn) measurement of Korover and the corresponding momentum distribution [47,50]. The Hall A signal to noise ratio was significantly worse than that expected in CLAS12.

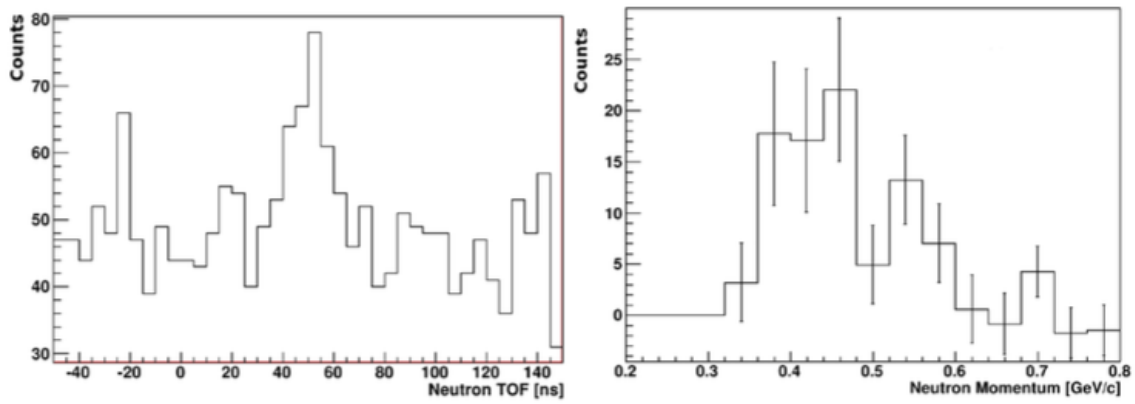

Figure 16: (left) The neutron time-of-flight measured in the Hall A 4He(e,e'pn) measurement of Korover, and (right) the corresponding accidentals-subtracted neutron momentum distribution [50].

We do see neutrons in the CLAS6 TOF for $75^o < \theta_n < 99^o$. Figure 17 shows the electron-TOF relative times for the EG2 run period. The photon peak, neutron peak and background levels can be clearly seen. The random background can be deduced from the number of events with TOF < 10 ns (left of the photon peak).

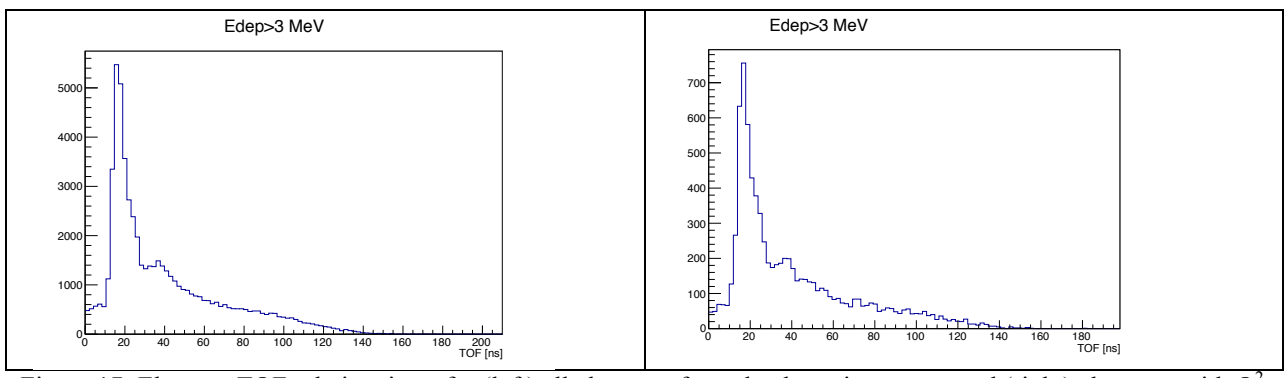

Figure 17: Electron-TOF relative times for (left) all electrons from the deuterium target and (right) electrons with $Q^2 > 2$ GeV^2 and W > 2 GeV for the EG2 run period for TOF counters between 35 and 43. The large peak at about 20 ns is the photon peak. The excess over background from 30 to 60 ns are the neutrons. The random background can be deduced from the number of events with TOF < 10 ns (left of the photon peak). The threshold for neutron detection was 3 MeVee.

The neutron momentum resolution depends on the distance, time resolution and neutron velocity. For detectors 2.5 meters from the target with our anticipated 200 ps time resolution, the momentum resolution for 300-500 MeV/c neutrons will be

$$\frac{\Delta p}{p} = \frac{\Delta TOF}{TOF} = \frac{0.2\text{ns}}{(25-17)\text{ns}} \approx 1\%$$

The actual resolution will be slightly worse at 2 m and slightly better at 3.5 m. The 6-cm detector thickness will add a momentum uncertainty of $\sigma_p = (0.06\text{m}/3.5\text{m})/\sqrt{12} = 0.5\%$.

The uncertainty in the determination of x' is shown below.

High x' kinematics	Low x' kinematics
$E' = 4.39 \pm 0.02$ GeV $\theta_e = 17^o \pm 0.057^o$ $\|p_s\| = 0.35 \pm 0.0035$ GeV/c $\theta_{sq} = 160^o \pm 1.5^o$ $x' = 0.503 \pm 0.007$ $W' = 2.18 \pm 0.024$ GeV	$E' = 4.39 \pm 0.02$ GeV $\theta_e = 13.5^o \pm 0.057^o$ $\|p_s\| = 0.35 \pm 0.0035$ GeV/c $\theta_{sq} = 160^o \pm 1.5^o$ $x' = 0.316 \pm 0.0046$ $W' = 2.518 \pm 0.02$ GeV

We plan to calibrate BAND during the experiment using the restricted $d(e,e'p\pi^+\pi^-)n$ and well-known quasielastic $d(e,e'p)n$ reactions.

Designing and building this detector will be a high priority of the MIT, Tel Aviv, UTFSM and ODU groups. The ODU group has made major hardware contributions to CLAS and CLAS12. The UTFSM has extensive detector experience and contributed about 4000 hand-polished lightguides to Hall D. The Tel Aviv group has extensive experience in designing, building and operating neutron detectors at BNL and at much higher luminosities in Hall A. The MIT group has extensive hardware experience and will commit significant resources to this project. We will seek external funding to build BAND from US and international funding agencies.

III.2.2 Experimental Acceptances

Fig. 18 shows the combined CLAS/BAND coverage in neutron momentum and angle between the neutron and the momentum transfer θ_{nq}. Fig. 19 shows the phase space coverage as a function of Q^2, x', W' and the spectator angle θ_{nq} and momentum p_n.

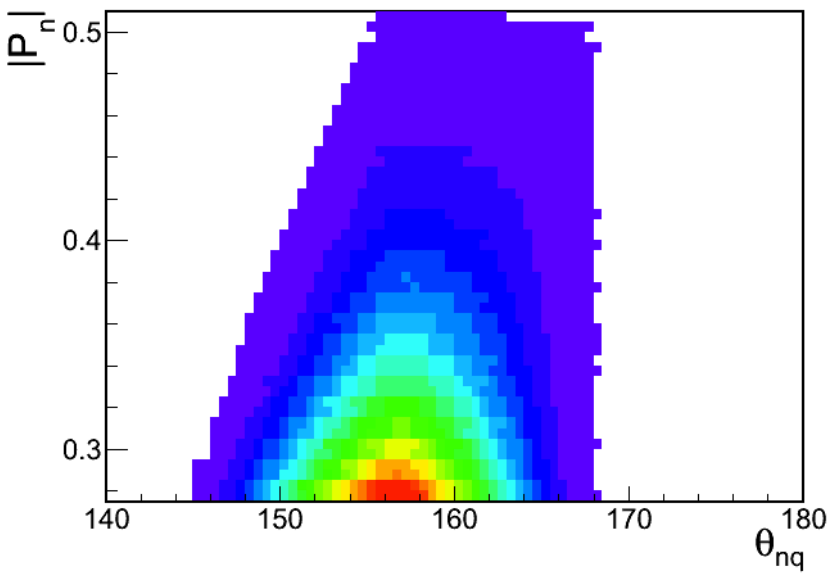

Figure 18: The BAND acceptance as a function of neutron momentum and angle between the neutron and the momentum transfer θ_{nq}. Events are distributed according to the cross section [40].

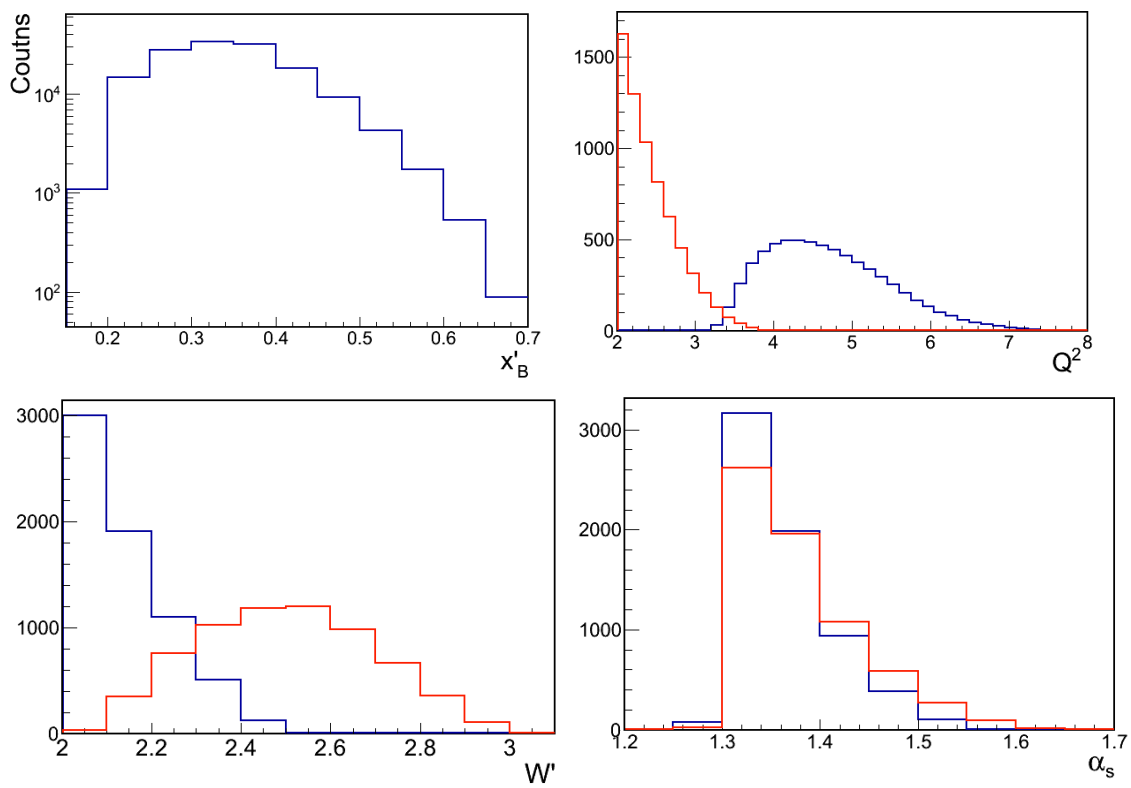

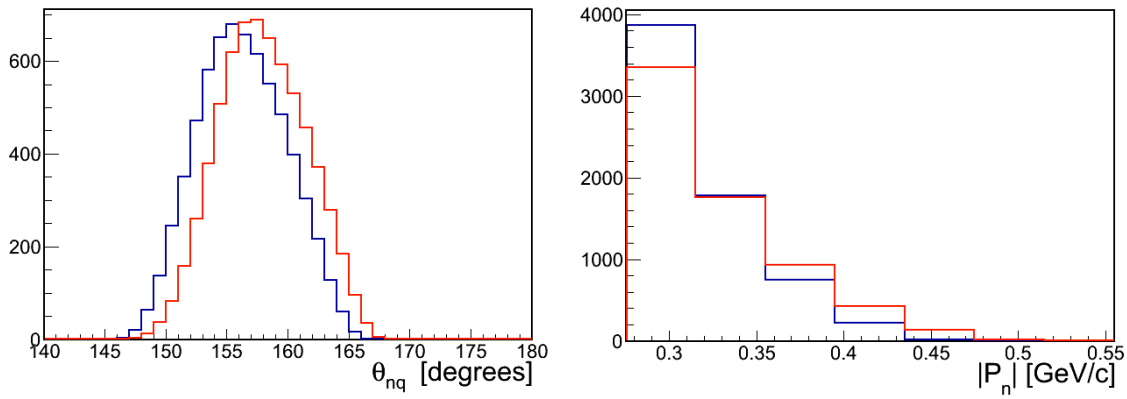

Figure 19: The phase space covered by the two proposed settings. The red and black curves show the low (0.25 – 0.35) and high (>0.5) *x*' bins respectively. All plots are normalized to the expected counts in the high-x' kinematics.

III.3 Rates

The signal and background rates were calculated by a simulation that took into account the kinematics and acceptance of the detectors using a luminosity of 10^{35} cm^{-2} sec^{-1}.

We calculated the differential cross sections $d^4\sigma / dE'_e d\Omega_e dT_s d\Omega_s$ using the PWIA model of Cosyn and Sargsian [40] for $d(e,e'n_s)$ for the proposed kinematics, in units of nb/sr^2-GeV^2. Note that the Cosyn/Sargsian PWIA cross section agrees closely with that of Ciofi degli Atti and collaborators [41]. Note also that the PWIA model should under predict the cross section at $\theta_{nq} \approx 90^o$ where we expect large Final State Interaction contributions. We stepped the electron and neutron momenta and angles through the appropriate acceptances and calculated the expected number of counts for each bin. We conservatively assumed ϕ coverage of 50% for the electron and 75% for the neutron.

The accidental coincidence rate will be about 20 times smaller in CLAS12 at $L = 10^{35}\,\text{cm}^{-2}\text{s}^{-1}$ than in the approved Hall C experiment at $L = 2\times10^{36}\,\text{cm}^{-2}\text{s}^{-1}$. This will improve our signal to noise ratio from 1:6 (worst case in Hall C) to between 2:1 and 1:1. The detailed background calculations are described in detail in Appendix B. In order to remove this background, we will create an electron-neutron relative time plot, sample the background using the off-time events, and subtract this background from the signal peak (see Fig. 16). By sampling the background extensively outside of the coincident neutron peak, we plan to reduce the statistical uncertainty from $\sqrt{S+2B}$ to $\sqrt{S+B}$.

Table 2 shows the number of semi-inclusive $d(e,e'n_s)$ events expected in 40 days of beam running with Run Group B as a function of α_s and as a function of momentum p_n for low and high x'. We anticipate taking 40 days of data with Run Group B and a further 8 equivalent days of data with Run Group F (BoNuS) and 35 equivalent days of data with Run Groups D and E. Table 3 shows the number of events for 75 days of beam time.

Table 2: Expected number of events for 40 days beam time with $d(e,e'n_s)$ for $Q^2 > 2$ GeV^2, $W' > 2$ GeV and $\theta_{ps} > 110^o$. The statistical uncertainty is indicated in parenthesis and includes the contribution of the random background subtraction, see Appendix B for details.

x' \ α_s	**1.3 – 1.35**	**1.35 – 1.4**	**1.4 – 1.45**	**1.45 – 1.5**	**1.5 – 1.55**	
0.25 < x' < 0.35	13,100 (1.2%)	10,000 (1.3%)	5500 (2.6%)	3000 (2.5%)	1400 (3.7%)	
x' > 0.5	1700 (3.5%)	1100 (6%)	500 (7.5%)	200 (11%)	55 (22%)	
x' \ $\lvert P_{recoil}\rvert$	**275 - 300**	**300 - 325**	**325 - 350**	**350 - 375**	**375 - 400**	**400 - 425**
0.25 < x' < 0.35	12,000 (1%)	7800 (1.8%)	5400 (1.8%)	3500 (2.5%)	2300 (3%)	1400 (3.5%)
x' > 0.5	1500 (4.3%)	1000 (6%)	550 (7.8%)	350 (9.5%)	200 (14%)	80 (19%)

Table 3: Expected number of events for 75 days beam time with $d(e,e'n_s)$ for $Q^2 > 2$ GeV^2, $W' > 2$ GeV and $\theta_{ps} > 110^o$. The statistical uncertainty is indicated in parenthesis and includes the contribution of the random background subtraction, see Appendix B for details.

x' \ α_s	**1.3 – 1.35**	**1.35 – 1.4**	**1.4 – 1.45**	**1.45 – 1.5**	**1.5 – 1.55**	
0.25 < x' < 0.35	24,500 (0.7%)	18,400 (0.9%)	10,150 (1.3%)	5,500 (1.6%)	2,560 (2.3%)	
x' > 0.5	3,200 (2%)	2,000 (3.4%)	940 (5%)	380 (7.3%)	100 (13%)	
x' \ $\lvert P_{recoil}\rvert$	**275 - 300**	**300 - 325**	**325 - 350**	**350 - 375**	**375 - 400**	**400 - 425**
0.25 < x' < 0.35	22,000 (0.7%)	14,500 (1%)	10,000 (1.3%)	6,600 (1.5%)	4,400 (1.9%)	2,600 (2.3%)
x' > 0.5	2,700 (2.0%)	1,750 (3.3%)	1,000 (4.9%)	600 (6.1%)	350 (8.3%)	150 (11.5%)

III.4 Extracting the in medium structure function

In order to extract the in-medium nucleon structure function ratio from the cross section ratio data, we need to reduce the uncertainties due to (1) The deuteron momentum distribution $n(p_s)$ is not well known at these large spectator momenta and (2) the FSI are not well known.

We estimate the current uncertainty due to the effects of FSI by comparing the ratio of cross sections at small and large x' calculated with and without FSI using the calculations that predict the largest FSI contributions at backward angles [41,42]. The difference between these two ratios is less than 4%. Although we expect to reduce that uncertainty as described below, we will use 4% as our interpretation uncertainty.

To reduce the uncertainties due to these effects, which vary strongly with W' and p_s, we will (a) measure cross sections over a wide kinematic range to provide data that will allow theorists to study the variation of the cross section with different variables, allowing them to optimize different ingredients of their calculations and (b) calculate ratios of cross sections so that most of the remaining theoretical uncertainties will cancel.

Effects from off shell nucleons should be small at low x'. We will fix p_s and x' to significantly reduce the uncertainty from the deuteron momentum distribution. Then we will vary W' to study how FSI varies with the invariant mass of the produced hadrons. Figure 20 shows the W' distribution for one bin in low x' and small p_s. Reproducing this data by the theoretical calculation is a strong test of its ability to describe FSI.

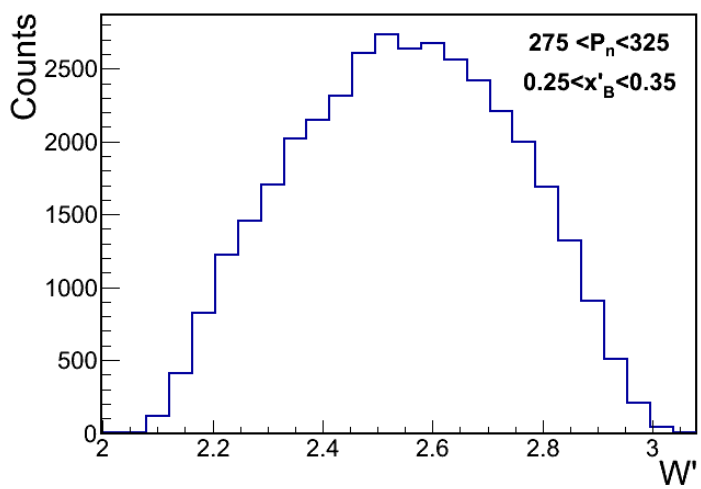

Figure 20: The expected $d(e,e'n_s)$ W' distribution for one bin in x' and recoil momentum, p_s.

Similarly, measuring the cross section at fixed x' and W' and varying p_s will help the theorists constrain the recoil momentum distribution used in their calculations (see Fig. 21).

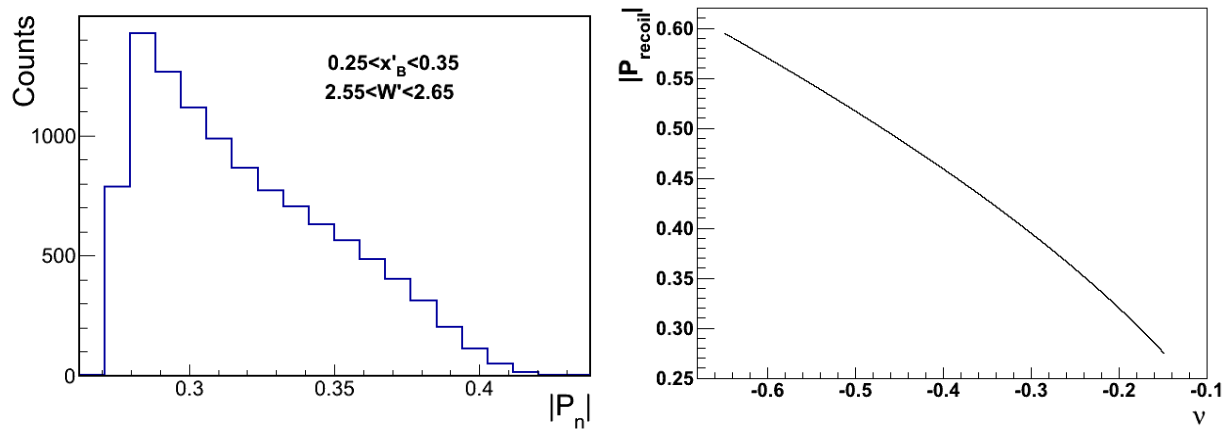

Figure 21: (left) The expected $d(e,e'p_s)$ recoil momentum (p_s) distribution for one bin in *W*' and *x*'. (right) The relationship between virtuality and recoil nucleon momentum.

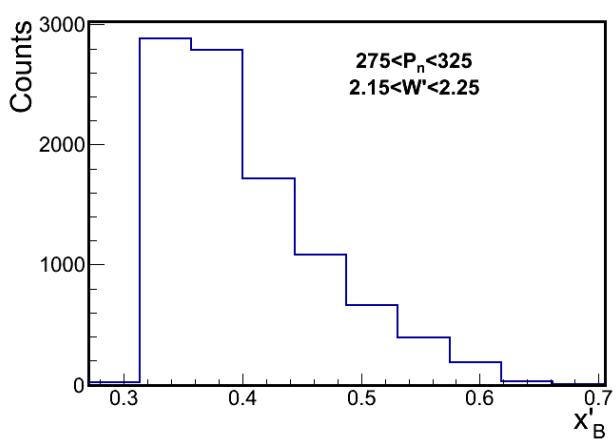

Figure 22: The expected $d(e,e'p_s)$ *x*' distribution for one bin at small p_s and *W*'. These conditions should minimize the uncertainty of both FSI and deuteron momentum distribution contributions, especially in the ratio of cross sections.

After optimizing the state of the art cross section calculations without nucleon modification at low *x*', we can look for off shell effects by fixing both *W*' and p_s and dividing the measured ratio of cross sections at high and low *x*' by the calculated ratio to get (Equation 1):

$$\left(\frac{d^4\sigma}{dx_1 dQ_1^2 d\vec{p}_s}\Big/\frac{d^4\sigma^{calc}}{dx_1 dQ_1^2 d\vec{p}_s}\right)\Big/\left(\frac{d^4\sigma}{dx_2 dQ_2^2 d\vec{p}_s}\Big/\frac{d^4\sigma^{calc}}{dx_2 dQ_2^2 d\vec{p}_s}\right)=$$

$$[F_2^*(x'_1,\alpha_s,p_T,Q_1^2)/F_2^*(x'_1,\alpha_s,p_T,Q_1^2)_{calc}]/[F_2^*(x'_2,\alpha_s,p_T,Q_2^2)/F_2^*(x'_2,\alpha_s,p_T,Q_2^2)_{calc}]$$

We will then plot this double ratio versus nucleon virtuality, versus spectator nucleon momentum, and versus spectator light cone momentum fraction α_s. The expected number of counts at small p_s and *W*' is shown in Figure 22.

The expected uncertainties for the ratio of the in-medium to free proton response function as calculated from the simulated data according to Eq. 1 are shown in Fig. 23 for 40 PAC days with Run Group B. The expected uncertainties for the full data taking period of 75 days are shown in Fig. 24. These uncertainties are much smaller than those of E12-11-107 (see Fig 12 right) for the proton.

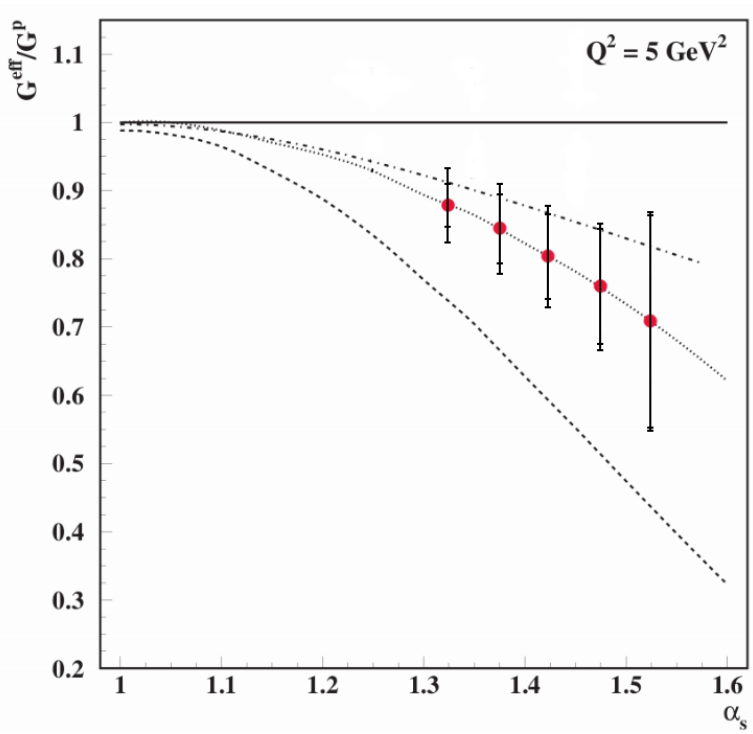

Figure 23: The α_s dependence of the modified proton response function ratio F_{2p}^{eff} / F_{2p} as in Fig. 8 with model predictions and simulated data including statistical (inner error bars) and systematical (outer error bars) uncertainties for 40 days of data. We expect an additional 4% interpretation uncertainty (see text for details). The label "Q^2 = 5 GeV^2" refers to the models, not the data.

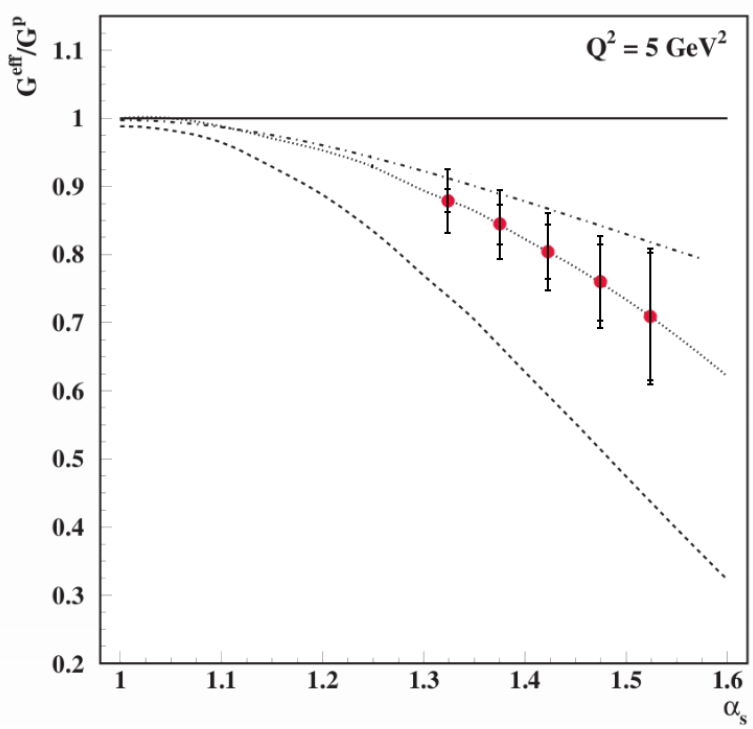

Figure 24: The same as Figure 23, but for 75 days of data. We expect an additional 4% interpretation uncertainty (see text for details). The label "Q^2 = 5 GeV^2" refers to the models, not the data.

The statistical uncertainties shown in Figures 23 and 24 include contributions from the signal and the random coincidence background. The statistical errors in the tables were estimated as $\sqrt{S+B}$ where S and B are the number of signal and background events in each bin. This is reasonable since the random background at backward angles should be a smooth function and will be oversampled and fit.

We will measure both absolute cross sections and ratios of cross sections. The absolute cross sections will primarily be used to understand systematic effects in both the detectors and the calculations. We will compare our measurements of $d(e,e')$ to the well-known inclusive $d(e,e')$ cross sections. Note that the total luminosity as well as much of the spectrometer acceptance effects will cancel in the ratio of the cross sections at different x'.

In addition to the luminosity and CLAS12 acceptance uncertainties, a third class of systematic uncertainty comes from the unknown acceptance and efficiency of the BAND. We plan to model the detector and to calibrate it. We will calibrate the neutron detection efficiency using the over-determined kinematically-complete $d(e,e'np)$ reaction where the electron and proton are detected by CLAS12 and the recoil neutron by the BAND. We estimate about 5% neutron detection uncertainty.

In summary, we estimate total 6% uncertainties in the measurement of the cross section ratios at low and high x'. We estimate a further contribution of 4% in the correction of this ratio for Final

State Interactions in order to extract F_2^{eff} / F_2, the ratio of the medium modified to free proton structure functions. This interpretation uncertainty is discussed in section III.4 above. For the cross section measurements (not ratios) we estimate the total statistical plus systematic uncertainty to be about 10%.

III.5 Measurement plan and Beam time request

We request to run in parallel with run groups F (BoNuS) and B (deuteron). They anticipate 80 PAC days of running in 2017-2018, but BoNuS will run at reduced luminosity, providing a total of 40+8=48 days of 10^{35} $cm^{-2}s^{-1}$ luminosity data. The BoNuS data will be valuable for understanding our coincidence backgrounds but will not significantly reduce our experimental uncertainties. Our first physics results will come from this data.

To improve statistics, we also request running in parallel with run groups E (Hadronization) and D (Color Transparency). They anticipate 70 days of running in 2019-2020, but the deuterium target will only provide half the luminosity.

When we run with the Hadronization and Color Transparency run groups, we plan to use BAND to simultaneously measure the tagged EMC effect, the ratio of the per-nucleon inclusive (e,e') cross sections on nucleus *A* relative to deuterium, tagged with a backward-going neutron.

III.6 Collaboration

The experimental group consists of people that were actively involved in exclusive measurements of high momentum transfer reaction in coincidence with recoil particles during the 6 GeV JLab program, either with the triple coincidence SRC measurements in Hall A (E01-015, and E07-006) or with the BONUS and DEEPS measurements in CLAS (E03-012, E94-102). This proposed experiment follows the same principle as the successfully completed 6 GeV experiments mentioned above and the collaboration has the needed expertise to perform the new experiment if approved.

The leading institutions have contributed to the construction of CLAS12 and have a vast experience in construction of large-acceptance neutron detectors. Specifically, resources from MIT, ODU and Tel-Aviv will be devoted to the construction of BAND.

In order to determine any possible changes in the nucleon structure function we need to collaborate extensively with theoreticians. The two theoretical groups that have contributed significantly to this proposal are C. Ciofi degli Atti and L. Kaptari as well as W. Cosyn and M. Sargsian. They anticipate participating in the interpretation of the data. Many other theoretical groups have expressed interest in the data and its interpretation. They are listed under the heading of "Theoretical Support" on the title page of this proposal.

We would like to thank the many people who proposed letters of intent and proposals to investigate this or similar physics. The proposals and LOIs include,

1. LOI12-07-012, Tagged Neutron Structure Function in Deuterium, S. Bueltmann, S. Kuhn and K. Griffioen
2. LOI 05-014, N. Liyanage and B. Wojtsekhowski

Appendix A: TAC Report on PR12-11-107

This proposal will measure spectator neutrons in DIS from deuterium with high precision and will thus complement the approved 12 GeV Hall C experiment which will measure spectator protons with high precision and spectator neutrons with reduced precision. Therefore, the theory review of experiment E12-11-107 is very relevant to this proposal and is reproduced below in its entirety.

PR12-11-107: In Medium Nucleon Structure Functions, SRC and the EMC effect

A.V. Radyushkin, M.R. Pennington

While by now the EMC effect has been observed in many experiments, and its possible origins a whole literature in itself, few new insights have been gained beyond a suggestion that part of the effect may be connected to short range correlations in the nucleus. This proposal marks an important attempt to actually differentiate between possible mechanisms (such as modification of the nucleon structure functions in the nuclear medium, and its relation to the nucleon virtuality) in a transparent way. The authors indicate that extraction of in-medium nucleon structure functions is theoretically complicated by the fact that the deuteron wave function is not well known at the large momenta corresponding to short range correlations, and that the final-state interactions are not precisely understood. However, several groups are engaged on studies that provide theoretical support for this proposal. The various frameworks discussed are not always consistent with each other. Consequently, the proponents need to differentiate between these approaches and set out what can be learnt in each case. Nevertheless, the depth of theory involvement is highly significant and one of the proposal's strengths. Such a level of commitment will need to be refreshed, later in this decade once the data have been taken, to ensure a robust interpretation of the results.

This is a well motivated experiment that has to be done, and one JLab is well placed to perform.

Appendix B: Random Coincidence Rate

The random d(e,e'n)X coincidence rate is estimated by multiplying three factors: (1) the single neutrons rate, (2) the inclusive d(e,e') rate, and (3) the coincidence time window. Fig. B1 shows the neutron detection efficiency as a function of scintillator energy threshold (in MeVee, MeV electron equivalent) for different neutron kinetic energies as simulated in Ref [51]. At our expected threshold of 3 MeVee, we are insensitive to 8 MeV neutrons and begin to be sensitive to 16 MeV neutrons. Fig. B2 shows Pavel Degtiarenko's single neutron rate calculation for a 1-uA electron beam passing through a 10-cm liquid deuterium target ($L = 6\times10^{36}\,\mathrm{cm}^{-2}\mathrm{s}^{-1}$). As part of the Hall-C LAD proposal, we determined that Pavel's calculations are consistent with our 6 GeV Hall C measurements of the backward singles neutron rates.

We used the rate of $4\times10^{5}\,\mathrm{s}^{-1}$ for $T_n > 15$ MeV neutrons passing through a 100% efficient 0.1 sr detector and scaled it by a factor of 60 for luminosity and detector solid angle and efficiency. We calculated the electron singles rates using the known inclusive d(e,e') cross-section and a luminosity of 10^{35} $\mathrm{sec}^{-1}\mathrm{cm}^{-2}$ over the CLAS acceptance for $5^{\circ} \le \theta_e \le 35^{\circ}$ and for $2 \le E'_e \le 8\,\mathrm{GeV}$ in fine bins. For each electron bin, we varied the neutron momentum and angle over the acceptance and calculated the appropriate kinematic variables (x, Q^2, x', W'). We calculated $\Delta CTOF$, the width of the coincidence time window, from the neutron momentum bin width. We then calculated the expected number of events in the bin using:

$$N = L\cdot\sigma_e\cdot\Delta\Omega_e\cdot\Delta E'_e\cdot F_n\cdot\Delta CTOF\cdot\Delta\Omega_n\cdot\epsilon\cdot T$$

where N is the number of background counts in the bin, $L = 10^{35}\,\mathrm{cm}^{-2}\mathrm{s}^{-1}$, σ_e is the inclusive d(e,e') cross section, $\Delta\Omega_e$ is the electron solid angle for the bin, $\Delta E'_e$ is the electron energy bin, $F_n = 6\times10^{4}\,\mathrm{Hz/sr}$ is the neutron flux, $\Delta\Omega_n$ is the neutron solid angle for the bin, $\epsilon = 0.3$ is the BAND neutron detection efficiency, and T is either 40 PAC days (for Run Group B) or 75 PAC days (for all run groups). We assumed the same ϕ coverage of 50% for the electron and 75% for the neutron as in our count rate estimates.

We validated the background calculation by comparing the accidental coincidence rates for a narrow bin in electron angle and momentum as calculated by our background calculation code and as calculated by hand using the single electron cross section and neutron rate.

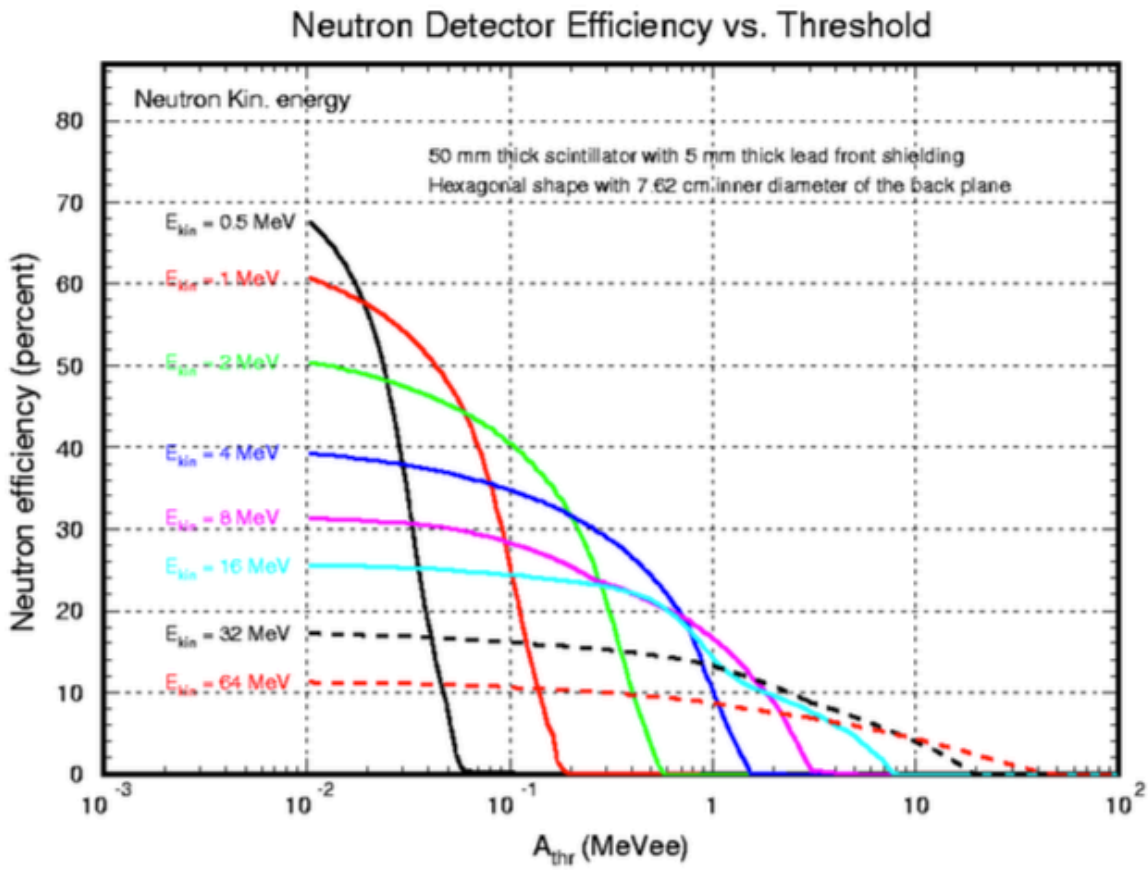

Figure B1: Neutron detection efficiency vs scintillator threshold in MeV electron equivalent (MeVee) [51].

Fig. B3 shows neutron background plotted vs $1/p$ and vs $\cos\theta_n$, showing that it is flat in both variables. The neutron background is flat in $1/p$ because the background in a given neutron bin is proportional to the time-of-flight width of that bin, which is proportional to $1/p$.

Fig. B4 shows the expected signal and background rate as determined by our simulations for 40 beam days. The rate is shown as a function of α_s for both our high- and low- x' kinematics. The signal-to-background ratios for the high-x' and low-x' kinematics are better than 2:1 and 4:1, respectively, for all α_s bins. We note that from past experience, non-target-related backgrounds are small compared to target-related backgrounds.

The variables W' and x' depend on both the electron and neutron kinematics, unlike W and x, which depend only on the electron. The electron acceptance for fixed W' and x' decreases dramatically with α_s and hence with neutron momentum. This causes the decrease of both signal and background with α_s seen in Fig. B4.

Experiments E07-006 and E01-015, conducted by our group in Hall-A, measured statistics of about 20 to 100 neutron events with typical signal-to-background ratios of about 1:3 – 1:4. The data from these measurements was successfully analyzed both using off-time background subtraction for count rate estimates and event mixing for kinematical distributions [proposal Ref.

22, 47]. The expected signal-to-background ratio in this proposal is considerably better (i.e. 2:1 vs. 1:3), and the overall statistics is much larger (e.g., by a factor of 10 to 100). Therefore, it should be much easier to identify the neutrons over the random background and extract the required signal.

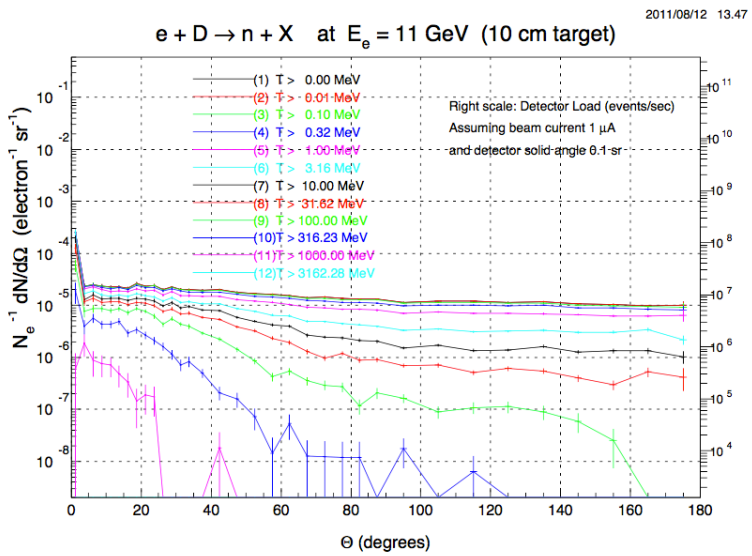

Fig. B2: Estimated neutron singles rates (right hand scale, Hz) for a 1-uA 11-GeV electron beam on a 10 cm long LD_2 target with a 100% efficient 0.1-sr neutron detector.

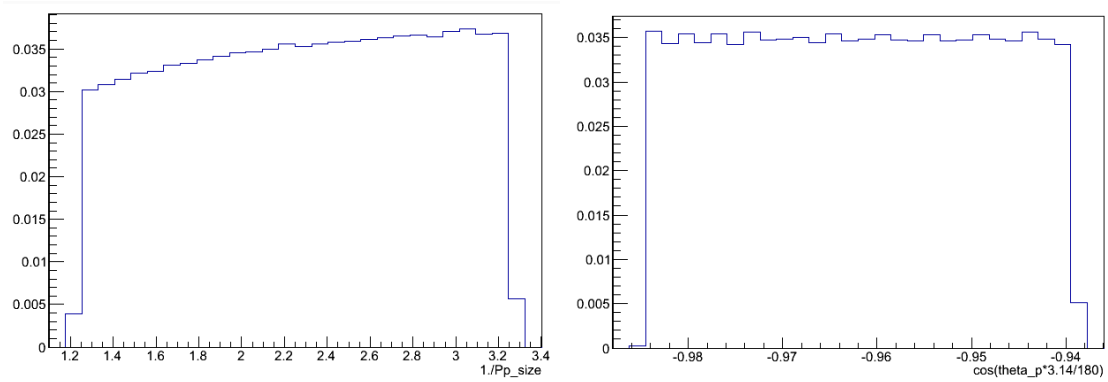

Fig. B3: The background neutron distribution plotted vs 1/p (left) and vs cos(theta) (right). The background is flat in 1/p because the amount of background in each bin is proportional to the TOF width of the bin.

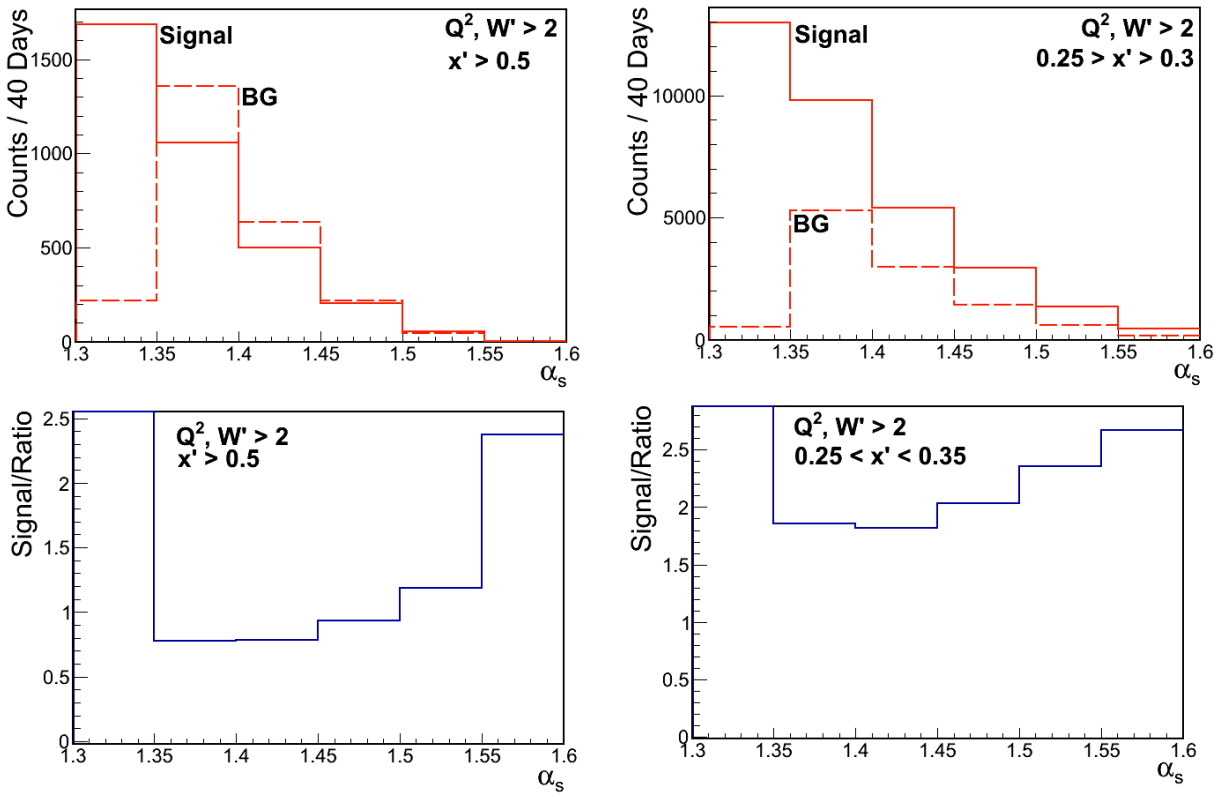

Fig. B4: (Top) Expected signal (solid) and background (dashed) counts for the d(e,e'n) reaction as a function of α_s, for Q^2>2 GeV^2, W'>2 GeV. The left and right plots show the high- and low-x' kinematics, respectively. (Bottom) The signal to background ratio for each bin in α_s. The signal to background ratio is off scale for the lowest α_s. The counts were calculated for the full CLAS12+BAND setup, assuming a luminosity of 10^{35} sec^{-1} cm^{-2} and 40 beam days. See text for details.

References

[1] J. J. Aubert *et al*., Phys. Lett. B **123**, 275 (1983).

[2] J. Ashman *et al*., Phys. Lett. B **202**, 603 (1988).

[3] J. Gomez *et al*., Phys. Rev. D **49**, 4348 (1994).

[4] M. Arneodo *et al*., Phys. Lett. B **211**, 493 (1988).

[5] M. Arneodo *et al*., Nucl. Phys. B **333**, 1 (1990).

[6] D. Allasia *et al*., Phys. Lett. B **249**, 366 (1990).

[7] J. Seely *et al*., Phys. Rev. Lett. **103**, 202301 (2009).

[8] D. F. Geesaman, K. Saito and A. W. Thomas, Ann. Rev. Nucl. Part. Sci. **45**, 337 (1995).

[9] P. R. Norton, Reports on Progress in Physics **66**, 1253 (2003).

[10] L. Frankfurt and M. Strikman, Phys. Rev. C **82**, 065203 (2010).

[11] S. A. Kulagin and R. Petti, Phys. Rev. C **82**, 054614 (2010).

[12] S. A. Kulagin and R. Petti, Nucl. Phys. A **765**, 126 (2006).

[13] M. Paolone, et *al*., Phys. Rev. Lett. **105**, 072001 (2010).

[14] A. De Shalit and H. Feshbach, Theoretical Nuclear Physics, Wiley, 1974.

[15] L.L. Frankfurt and M.I. Strikman, Phys. Rep. **76**, 215 (1981).

[16] L.L. Frankfurt and M.I. Strikman, Phys. Rep. **160**, 235 (1988).

[17] K.S. Egiyan *et al*., Phys. Rev. C **68**, 014313 (2003).

[18] K.S. Egiyan *et al*., Phys. Rev. Lett. **96**, 082501 (2006).

[19] The E01-015 Experiments Website, http://hallaweb.jlab.org/experiment/E01-015.

[20] E. Piasetzky, W. Bertozzi, J. W. Watson, and S. A. Wood (spokespersons) JLab experiment E01-15 (2001).

[21] R. Shneor *et al*., Phys. Rev. Lett. **99**, 072501 (2007), nucl-ex/0703023.

[22] R. Subedi *et al*., Science **320**, 1426 (2008).

[23] R. A. Niyazov *et al*. (CLAS Collaboration), Phys. Rev. Lett. **92**, 052303 (2004).

[24] H. Baghdasaryan *et al*., (CLAS Collaboration), Phys. Rev. Lett. **105**, 222501 (2010).

[25] J. L. S. Aclander *et al*., Phys. Lett. B **453**, 211 (1999).

[26] A. Malki *et al*., Phys. Rev. C **65**, 015207 (2001).

[27] A. Tang *et al*., Phys. Rev. Lett. **90**, 042301 (2003).

[28] E. Piasetzky *et al*., Phys. Rev. Lett. **97**, 162504 (2006).

[29] L. B. Weinstein, E. Piasetzky, D. W. Higinbotham, J. Gomez, O. Hen, and R. Shneor, Phys. Rev. Lett. **106**, 052301 (2011).

[30] L.L. Frankfurt and M.I. Strikman, Nucl.Phys. **B250**, 143 (1985); and Phys. Rep. **160**, 235 (1988).

[31] A.V. Klimenko *et al.* (The CLAS Collaboration), Phys. Rev. C **73**, 035212 (2006).

[32] H. Fenker, C. Keppel, S. Kuhn and W. Melnitchouk, Jefferson Lab Experiment E03-012, "The structure of the free neutron via spectator tagging."

[33] S. Bueltmann *et al*., Jefferson Lab Experiment E12-06-113, "The Structure of the Free Neutron at Large x-Bjorken."

[34] W. Melnitchouk, M. Sargsian, and M.I. Strikman, Z. Phys. **A359** (1997) 99.

[35] W. Melnitchouk, A. W. Schreiber, and A. W. Thomas, Phys. Rev. D **49**, 1183 (1994).

[36] W. Melnitchouk, A. Schreiber, and A. W. Thomas, Phys. Lett. B **335**, 11 (1994).

[37] F. Gross and S. Liuti, Phys. Rev. C **45**, 1374 (1992).

[38] S. Liuti and F. Gross, Physics Letters B **356**, 157 (1995).

[39] S. Kuhn, S. Bultmann, and K. Griffioen, Tagged Neutron Structure Function in Deuterium ("Deeps12"), Jefferson Lab Letter of Intent 12-07-102.

[40] W. Cosyn and M .Sargsian, Phys. Rev. C **84**, 014601 (2011) and private communication.

[41] C. Ciofi degli Atti and L. P. Kaptari, Phys. Rev. C **83,** 044602 (2011) and private communication.

[42] V. Palli, C. Ciofi degli Atti, L. P. Kaptari, C. B. Mezzetti and M. Alvioli, Phys. Rev. C **80**, 054610 (2009).

[43] "Nuclear Physics Comparative Research Review for the U. S. DOE", October 31 2013. http://science.energy.gov/~/media/np/pdf/Comparative%20Review/NP_Comparative_Research_Review_Report.pdf

[44] S. Brodsky *et al.*, "QCD and Hadronic Physics", Report on the QCD Town Meeting, arXiv: 1502.05728.

[45] J. Dudek et al., Eur. Phys. J. A **48,** 187 (2012), "Physics Opportunities with the 12GeV upgrade at Jefferson Lab", arXiv: 1208.1244.

[46] http://hallaweb.jlab.org/experiment/E01-015/documents/report.ps

[47] I. Korover *et al*. (Jefferson Lab Hall A Collaboration), Phys. Rev. Lett. **113**, 022501 (2014).

[48] O. Hen *et al*., Science **346**, 614 (2014).

[49] O. Hen, E. Piasetzky, and L. B. Weinstein, Phys. Rev. C 85, 047301 (2012).

[50] I. Korover, PhD thesis Tel Aviv University 2015, https://misportal.jlab.org/ul/publications/view_pub.cfm?pub_id=13735.

[51] Neutron Tagged Bound Proton Structure to Probe the Origin of the EMC Effect, N. Liyanage et al, Jefferson Lab PR05-014, 2015.